

**FATIGUE LIFE ANALYSIS OF A STEEL TRAPEZOIDAL BOX GIRDER  
BRIDGE USING MEASURED STRAINS**

by

Jose Soto Fuentes

A thesis submitted to the Faculty of the University of Delaware in partial fulfillment of the requirements for the degree of Master of Civil Engineering

Spring 2011

Copyright 2011 Jose Soto Fuentes  
All Rights Reserved

**FATIGUE LIFE ANALYSIS OF A STEEL TRAPEZOIDAL BOX GIRDER  
BRIDGE USING MEASURED STRAINS**

by  
Jose Soto Fuentes

Approved: \_\_\_\_\_  
Harry W. Shenton III, Ph.D.  
Professor in charge of thesis on behalf of the Advisory Committee

Approved: \_\_\_\_\_  
Harry W. Shenton III, Ph.D.  
Chair of the Department of Civil and Environmental Engineering

Approved: \_\_\_\_\_  
Michael J. Chajes, Ph.D.  
Dean of the College of Engineering

Approved: \_\_\_\_\_  
Charles G. Riordan, Ph.D.  
Vice Provost for Graduate and Professional Education

## **ACKNOWLEDGMENTS**

I would like to express my appreciation to everyone who helped me throughout this research project. Special thanks go to my advisor Dr. Harry “Tripp” Shenton not only for his guidance during this project, but throughout my graduate school experience at the University of Delaware. His willingness to directly get involved with the instrumentation at the bridge site was much valued. Additional thanks go to Danny Richardson and Michael Davidson for their assistance during the in-service monitoring of the Newport Viaduct. Lastly, I would like to thank DeIDOT for sponsoring this research project.

## TABLE OF CONTENTS

LIST OF TABLES .....	vi
LIST OF FIGURES .....	vii
ABSTRACT .....	x
 Chapter	
1 INTRODUCTION .....	1
1.1 Background.....	1
1.2 Previous Work.....	5
1.2.1 Kucz (2009).....	5
1.2.2 Quiqley (2009) .....	6
1.3 Objective and Scope of Current Work .....	8
1.4 Literature Review on Fatigue Analysis using Field Instrumentation .....	8
1.4.1 Zhou (2006).....	8
1.4.2 Connor and Fisher (2006).....	11
1.4.3 Alampalli and Lund (2006).....	13
1.5 Overview of Approach .....	14
1.6 Thesis Outline.....	16
2 FINITE ELEMENT MODELING .....	17
2.1 Model Description .....	17
2.1.1 Top Connection Model.....	21
2.1.2 Bottom Connection Model .....	21
2.1.3 Model Loading .....	22
2.2 Boundary Condition Study .....	23
2.3 Finite Element Analysis Results.....	26
3 IN-SERVICE MONITORING .....	33
3.1 Overview .....	33

3.2	Monitoring System .....	34
3.2.1	Datalogger .....	34
3.2.2	Strain Gages .....	35
3.2.3	Cellular Modem.....	38
3.3	CR500 Datalogger Programming.....	40
3.3.1	RTDAQ Software.....	40
3.3.2	Measurements.....	40
3.3.3	Power Consumption Estimates.....	42
3.4	Instrumentation Plan.....	46
3.5	Field Setup.....	47
3.6	Data Recorded .....	53
3.6.1	Extreme Event Snapshots.....	60
4	FATIGUE LIFE ANALYSIS.....	66
4.1	Methodology.....	66
4.2	Stress at Weld Toe.....	67
4.3	Effective Stress ( $S_r$ ).....	70
4.4	Lifetime Average Daily Truck Traffic (LADTT) .....	73
4.5	Mean Fatigue Life Estimates.....	75
5	CONCLUSIONS AND RECOMMENDATIONS.....	82
5.1	Summary and Conclusions.....	82
5.2	Recommendations .....	87
	REFERENCES.....	88
	APPENDIX A. FINITE ELEMENT ANALYSIS OUTPUT.....	90
	APPENDIX B. RTDAQ PROGRAMMING CODE.....	97
	APPENDIX C. HISTROGRAMS AND DATA PLOTS .....	106

## LIST OF TABLES

Table 2.1	Summary of loading and boundary condition cases analyzed.....	26
Table 2.2	Boundary condition study results. All values in ksi. ....	30
Table 2.3	Individual bolt hole loading results for top connection plate. ....	31
Table 3.1	Current consumption estimates for the monitoring system. ....	45
Table 3.2	Rainflow histogram results for BDI transducers .....	55
Table 3.3	Rainflow histogram results for foil gages .....	56
Table 4.1	Nodal stress ( $\sigma_y$ ) values obtained along superimposed foil gage length. ....	69
Table 4.2	Stress ( $\sigma_y$ ) at superimposed foil gage location and corresponding weld toe maximum stress ( $\sigma_y$ ) for varying boundary conditions. ....	70
Table 4.3	Effective Stress calculation results. ....	72
Table 4.4	LADTT estimates with 4% exponential growth rate.....	74
Table 4.5	ADTT lane reduction factor from FEESB (AASHTO, 1990).....	76
Table 4.6	Fatigue life calculations.....	77
Table 4.7	Fatigue life estimates.....	80

## LIST OF FIGURES

Figure 1.1	Aerial view of Newport Viaduct. (Yahoo Maps, 2011).....	2
Figure 1.2	Type E diaphragm (Quiqley, 2009).....	4
Figure 1.3	Typical condition of fatigue cracking at Type E diaphragm locations (DMJM Harris, 2006) .....	4
Figure 1.4	Stress range versus number of cycles. (Zhou, 2006).....	10
Figure 1.5	Example of extrapolated stresses (Connor & Fisher, 2006).....	12
Figure 2.1	Tetrahedral element with 10 nodes and four integration points. (ABAQUS, 2008).....	18
Figure 2.2	Bethlehem Steel fabrication drawings of Type E diaphragms. (Courtesy of DelDOT) .....	20
Figure 2.3	Localized top connection model. Notice higher mesh density in web gap region. ....	21
Figure 2.4	Localized bottom connection model. Notice higher mesh density in web gap region. ....	22
Figure 2.5	Loading on the inside surface of the bolt holes.....	23
Figure 2.6	Boundary condition cases for the top connection model. ....	24
Figure 2.7	Bottom connection, bottom edge fixed analysis results. Maximum principal stress concentrations are highly localized near web gap region.....	28
Figure 2.8	Top connection, top edge fixed. Maximum principal stress concentrations are highly localized near web gap region.....	29
Figure 2.9	Top connection, top edge fixed zoomed in view. Maximum principal stress gradient becomes extreme near weld toe. ....	29
Figure 3.1	CR5000 data logger with 120VAC adapter and PCMCIA data card. ....	35

Figure 3.2	BDI strain transducer ST-350. ....	37
Figure 3.3	Quarter bridge Micro-Measurements foil gage.....	37
Figure 3.4	Campbell Scientific Terminal Input Modules to be used with foil gages/.....	38
Figure 3.5	Raven XTV cellular modem and Omni Directional Antenna .....	39
Figure 3.6	Program Generator module within RTDAQ. A summary of the output tables is shown. ....	41
Figure 3.7	One of two 12V batteries used to power the monitoring system. ....	43
Figure 3.8	Strain gage instrumentation plan.....	47
Figure 3.9	Location where monitoring system was installed. (DelDOT, 1972).....	48
Figure 3.10	DelDOT bucket truck used to reach access hole above Ayre Street.....	49
Figure 3.11	Installation of foil gage #2 on top web gap region.....	50
Figure 3.12	BDI transducers clamped to the bolted legs of cross frame angles.....	50
Figure 3.13	View of strain transducers and foil gage after installation.....	51
Figure 3.14	Final wiring of monitoring system. ....	52
Figure 3.15	Rainflow histogram for foil gage #1, bins 2-5. ....	57
Figure 3.16	Rainflow histogram for foil gage #1, bins 6-30. ....	58
Figure 3.17	Averaged maximum/minimum recordings for BDI 2171 .....	59
Figure 3.18	Averaged data recorded for BDI 2171 at 100Hz.....	60
Figure 3.19	Snapshot event #1 cross frame gages. ....	61
Figure 3.20	Snapshot event #1 mid-web and bottom flange gages. ....	61
Figure 3.21	Snapshot event #1 web gap foil gages #1 & #2. ....	62
Figure 3.22	Snapshot event #1 BDI gages adjacent to connection plate.....	62
Figure 3.23	Snapshot event #2 cross frame gages. ....	63

Figure 3.24	Snapshot event #2 mid-web and bottom flange gages. ....	64
Figure 3.25	Snapshot event #2 web gap foil gages #1 & #2. ....	64
Figure 3.26	Snapshot event #2 BDI gages adjacent to connection plate. ....	65
Figure 4.1	Foil gage #1 field location superimposed on bottom web gap finite element model. ....	68

## **ABSTRACT**

The Newport Viaduct is a 1,984 feet long bridge owned by the Delaware Department of Transportation located in Newport, DE. During an in-depth inspection in 2006, approximately 665 cracks were discovered near the internal cross frame diaphragm connection plates and the girder webs. A 2.5 inch gap exists between the termination of the diaphragm connection plate and the flanges of the girder. This is a known fatigue prone detail subject to out of plane deformations which lead to the formation of distortion induced fatigue cracks.

Previous research done on the Newport Viaduct used global finite element models to estimate the fatigue life of the web gap details and analyze potential retrofit options. The purpose of this project is to measure site specific strains caused by variable traffic loads and use this data to carry out a fatigue life analysis of the web gap details.

In order to assist in the fatigue life analysis, localized finite element models of the web gap details were created. Given geometric differences, separate models were created for the top and bottom web gap details. The finite element models were created using FEMAP and solved using ABAQUS. The analysis results showed a high stress gradient in the web gap region with a maximum near the weld toe. Moreover, the results showed that the bottom web gap detail experienced higher stresses than the top web gap detail given the same loading.

In-service monitoring of the Newport Viaduct was carried out for 23 days. Resistive foil type strain gages were installed directly in the top and bottom web gap

regions and data was collected and processed at 100Hz using the Rainflow algorithm to count the number of load cycles and their magnitude. The recorded data was used in conjunction with the bottom web gap finite element model and Miner's Rule to determine an effective stress at the weld toe.

The results predict a mean fatigue life of 22 years for the bottom web gap detail. Furthermore, current uncracked web gap details are expected to crack in the future.

## **Chapter 1**

### **INTRODUCTION**

#### **1.1 Background**

The Newport Viaduct is a trapezoidal box girder bridge owned by the Delaware Department of Transportation (DelDOT) located in Newport, DE. Bridge 1-501, as it is also known consists of 19 spans and carries four lanes of traffic of State Route 141 over Route-4, local streets, Amtrak rail tracks and the Christina river. The Newport Viaduct was built in 1978 and its overall length is approximately 1,984 feet. According to figures provided by DelDOT, average daily traffic (ADT) was 69,412 in 2007 for both directions with an estimated 9% truck traffic (Kucz, 2009). Figure 1.1 on the next page shows an aerial image of the Newport Viaduct location.

The cross section of the Newport Viaduct varies from two to four trapezoidal steel box girders in each direction depending on the span. The trapezoidal box girders are approximately 4 feet deep and 10 feet wide, measured from the centerline of the webs. The northbound and southbound structures act independently given an open joint located between them. Grade 36 steel ( $f_y=36$  ksi) is used throughout the steel girders except in the negative moment regions where grade 50 ( $f_y=50$ ksi) is used. Shear studs are welded to the top flange to achieve composite action with the concrete deck. The composite concrete deck is cast in place with a 28-day specified strength of 4,500 psi. A more extensive description of the bridge structure can be found in Kucz, 2009.

In 2006 the consulting firm AECOM conducted an in-depth inspection of the Newport Viaduct and discovered 665 cracks near the connection plates of the Type E internal diaphragms. Moreover, during an interim inspection in 2009 the number of cracks detected inside the trapezoidal box girders had increased to 1,648. These cracks ranged in length from 1/8" to 4" and occurred on both sides of the diaphragm connection plates. In order to analyze the cause of these cracks and to study potential retrofit options, a research joint venture was formed between DelDOT, AECOM and the University of Delaware.

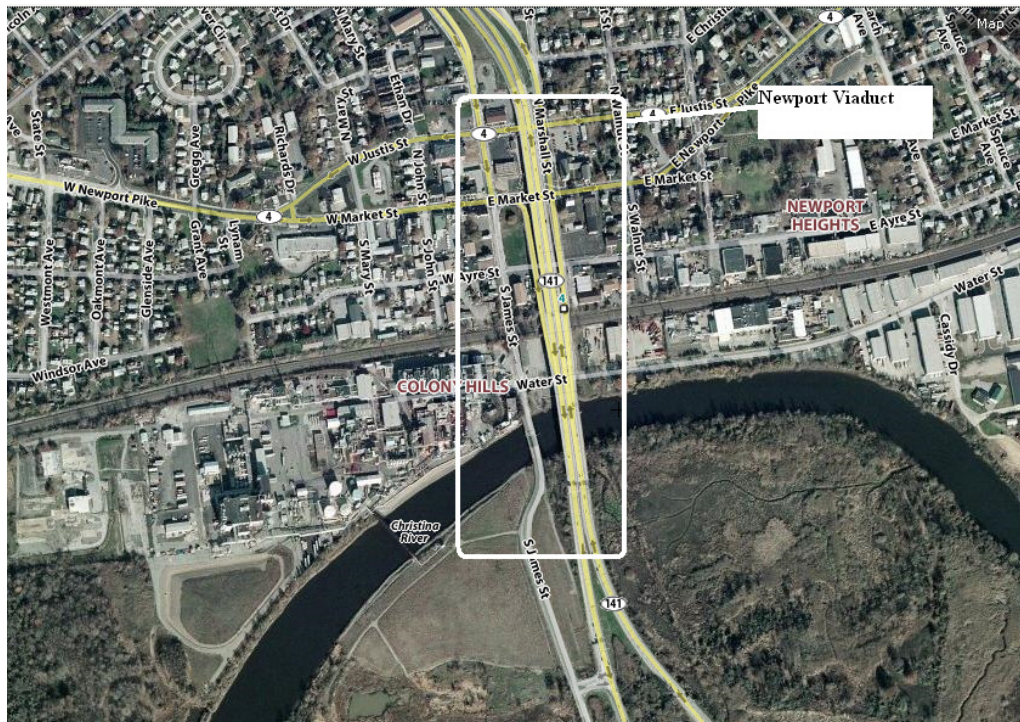


**Figure 1.1** Aerial view of Newport Viaduct. (Yahoo Maps, 2011)

The cracks that were uncovered during the in-depth inspection were all located near Type E internal diaphragms. These diaphragms consist of two 3"x3"x $\frac{3}{8}$ " angles welded to  $\frac{3}{8}$ " thick connection plates which in turn are welded to the web of the girders. These connection plates are not attached to the top or bottom flanges of the girder, as it was common practice to avoid transverse welds on the tension flange in steel bridges built prior to the late 1970s (Zhou, 2006). As a result, a 2.5" gap exists between the termination of the connection plate and the top and bottom flanges of the girder. This web gap region is a known fatigue prone detail which is avoided altogether in current design codes. The AASHTO LRFD Bridge Design Specifications states that "connection plates are to be rigidly attached to all components of a plate girder" (AASHTO, 2010). Figure 1.2 on the next page shows a typical Type E internal diaphragm with fatigue crack locations.

The lack of continuous rigid attachment of the connection plate together with the lateral forces transferred from the cross frames have caused out of plane deformations in the web gap region. It is a common fact that the smaller the depth of the web gap, the greater the distortion induced stress (Zhou, 2006). These deformations induce secondary stresses at the weld toe of the connection plates and have lead to the formation and propagation fatigue cracks near the Type E. This type of fatigue cracking is known in the literature as distortion induced fatigue cracking. A complete review of distortion induced fatigue cracking can be found in Kucz, 2009. Figure 1.3 on the next page shows the distortion induced fatigue cracks at the Type E diaphragm locations.

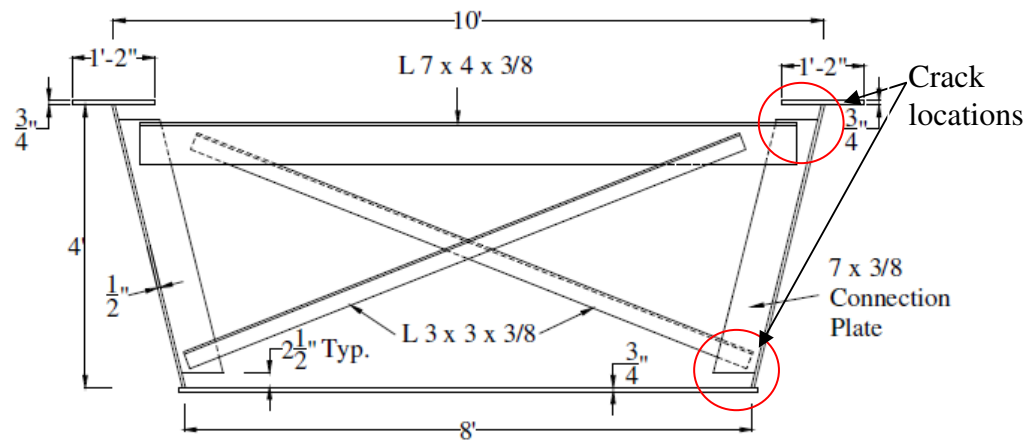


**Figure 1.2** Type E diaphragm (Quiqley, 2009).

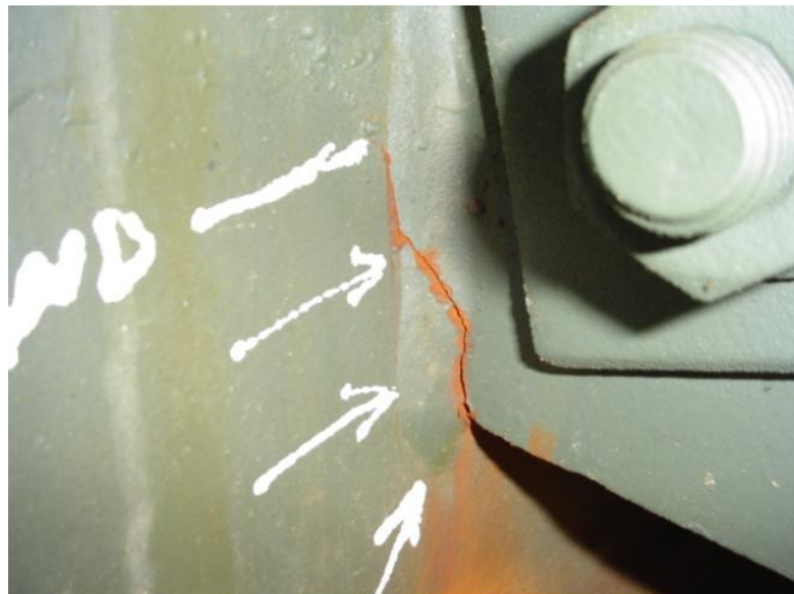


**Figure 1.3** Typical condition of fatigue cracking at Type E diaphragm locations (DMJM Harris, 2006)

## **1.2 Previous Work**

In 2009, two University of Delaware Masters Theses were completed on the Newport Viaduct. Kucz (Kucz, 2009) constructed a finite element model of spans 9, 10 and 11 and used it to obtain stresses at the weld toe and perform a fatigue life analysis. A field calibration test with known vehicle weights was carried out to validate the accuracy of the finite element model. Quiqley (Quiqley, 2009) created a finite element model of spans 12-16 to study potential retrofit options. A field test with known vehicle weights was also conducted to validate the finite element model. In total three different retrofit possibilities were analyzed.

### **1.2.1 Kucz (2009)**

The goal of this thesis was to perform fatigue life analysis of the Newport Viaduct. For this purpose, a finite element model of spans 9-11 was created in FEMAP and subsequently analyzed in ABAQUS. The model consisted of reduced shell integration elements (SR3, SR4) for the bridge and beam elements (B31) for the cross frames. Boundary conditions such as bearings and supports were modeled accordingly by restricting degrees of freedom of appropriate nodes. This finite element model was used to determine the stress range at the weld toe for a given fatigue truck loading. This was accomplished by applying the wheel loads of the 54 kip AASHTO fatigue truck on the bridge deck. To simulate the vehicle moving along the bridge, these wheel loads were advanced along the bridge in 2 ft. intervals. Overall, the model consisted of 160,135 elements and 165,733 nodes.

To ensure the accuracy of the finite element model, a field test was performed. On December 17, 2008 with aid of DelDOT personnel, several locations in span 10 southbound were instrumented with 23 BDI strain transducers and vehicles of

known weight were driven over the selected spans. While generally accurate, the results of the calibration test show poor agreement between computed and measured stresses for the cross frame angles. This could have been caused because the BDI transducers were installed on the un-bolted angle leg and shear lag effects might have been present. On the other hand, relatively good correlation was found between the computed and measured stresses in the bottom flange. Ultimately, the finite element model created was used to determine the stress range used in the fatigue life analysis.

Following the procedure outlined in AASHTO's Guide Specifications For Fatigue Evaluation of Existing Steel Bridges (FEESB) (AASHTO, 1990) a remaining fatigue life analysis was performed. Lifetime average daily truck traffic was estimated using a combination of known ADT and historical growth rates. The results of the fatigue life analysis show that web gap regions do not possess infinite fatigue life and they are expected to exhibit fatigue crack formation approximately 27-32 years after construction. Given the cracks detected in the 2006 inspection and that the Newport Viaduct has a service life of 33 years in 2011, these results are not unreasonable.

### **1.2.2 Quiqley (2009)**

The overall goal of this thesis was to model various retrofits options and evaluate their effectiveness at reducing the stresses at the weld toe of the web gap. A finite element model of spans 12-16 southbound was created in FEMAP and analyzed using ABAQUS. Four noded shell elements (SR4) were used to model the bridge, while beam elements (B31) were used for the cross frames. Boundary conditions were taken from bridge plans and modeled accordingly by limiting translation/displacement degrees of freedom at appropriate nodal locations.

A field test was performed on December 17, 2008 to validate the accuracy of the finite element model created. 23 BDI strain transducers were installed throughout span 15 southbound and vehicles of known weight made passes on the bridge. Unfortunately, a poor correlation was found between the finite element model and the recorded field data. To overcome this drawback, the finite element model created by Dan Kucz for spans 9-11 was used to model the retrofit options.

Three potential retrofit options were analyzed. Positive attachment of the connection plate to the flanges was the first option considered. The lightest section satisfying the stiffness requirements set by Fisher & Keating (Fisher and Keating, 1989) was a WT 12x88. This WT section could be bolted to the bottom flange, but it would have to be welded to the top flange given the presence of the concrete deck. The second option considered was the slot retrofit. The idea behind this repair was to lengthen the web gap, thus reducing the out-of-plane stresses generated at the weld toe. In order to accomplish this, the connection plate would have to be flame cut so that the new web gap exceeds a Fisher recommended length of 11.8 inches. The third option considered was the removal of the Type E diaphragm's cross frames. This should significantly reduce the stress transferred to the connection plates and the out-of-plane deformation in the web gap region. However, considerations need to be given to the overall structural integrity of the bridge and any potential increase in bending stresses of the box girders.

Finite element analyses were done for each of the retrofit options and their results were compared to the original bridge structure without retrofits. It was found that providing four bolts for each WT attachment reduced the web gap stresses by 64%-79%. The slot retrofit option resulted in a significant decrease in the stresses in

the web gap region. Increasing the web gap length to 12 inches, leads to a stress reduction of 57%-77%. Lastly, the removal of the cross frame lead to a reduction of the stresses in the web gap region. It was found that stresses were reduced by 52%-94% simply by removing the cross frames. However, it was also found that the bottom flange stresses of the box girders would increase by approximately 20%. In conclusion, it was found that the all three retrofits could potentially reduce the stresses at the weld toe below the constant amplitude fatigue threshold.

### **1.3 Objective and Scope of Current Work**

The objective of this research project is to investigate the fatigue life of the Newport Viaduct using measured strains obtained from the site specific traffic. To accomplish this, a strain gage monitoring system was installed at the bridge site and relevant data was collected over 23 days. The recorded strain data was used in conjunction with localized finite element models to determine the effective stress at the weld toe in the web gap region. Additionally, the recorded data provided the number of load cycles the structure experiences. Lastly, the procedures outlined in AASHTO's FEESB were used to determine the mean fatigue of the web gap details.

### **1.4 Literature Review on Fatigue Analysis using Field Instrumentation**

#### **1.4.1 Zhou (2006)**

Zhou proposes a methodology for evaluating the remaining fatigue life of a bridge using field strain measurements. Instead of focusing on specification loads and distribution factors to calculate the stress range for a given structural detail, Zhou greatly favors using field strain measurements as they prove more accurate and can account for the effect of localized stresses.

The fatigue strength of a structural component is related to the stress range (S) and the number of load cycles (N) it experiences. Structural details are categorized by their S-N curve or AASHTO Fatigue Curves as A, B, B', C, C', D, E and E' based on their fatigue strength. Category A has the highest fatigue strength, while Category E' has the lowest fatigue strength. These S-N curves “are based on a lower-bound regression analysis of the test data with a 2.3% probability of failure” (Zhou, 2006). Each fatigue category has a lower stress range threshold for which fatigue cracking will never occur, regardless of the number of cycles the detail experiences. This is known as the Constant Amplitude Fatigue Threshold (CAFT). The web gap details near the Type E diaphragms at the Newport Viaduct are considered to be Category C detail with a CAFT of 10 ksi. Figure 1.4 on the next page shows the AASHTO Fatigue Curves.

Given that the S-N curves were developed for constant amplitude loading, it becomes necessary to determine an “effective” stress range from the variable amplitude loading a bridge experiences. Miner’s rule has been commonly used for this purpose; it extracts an effective stress range from a variable amplitude loading by calculating the cube root of the mean cube of all stress ranges. Zhou recommends using a cutoff value of  $0.5CAFT$  when calculating effective stresses. Miner’s rule will be used in Chapter 4 to compute effective stress ranges used in fatigue life analysis.

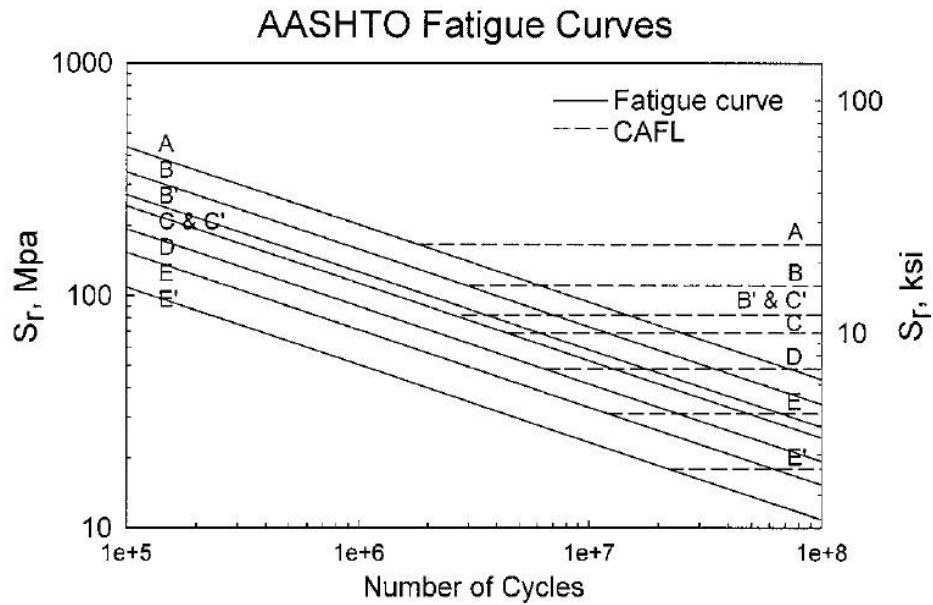


**Figure 1.4** Stress range versus number of cycles. (Zhou, 2006)

Zhou provides some key recommendations to be employed when performing the field monitoring of a bridge. First, prior to field strain measurement a structural analysis using computer models should be carried out to aid in the choosing of the strain gage locations. This should be done in order to avoid installing strain gages on members that experience primarily compression, as they will not control the fatigue life of a bridge. A calibration test should be performed at the beginning of the monitoring period once the strain gages are installed. The bridge should be closed to traffic and a truck of known weight should make passes on every lane. This will help in understanding the structural response of the bridge for a known load and establish baseline readings for all sensors. In order to capture normal traffic loads, the minimum monitoring period should be seven consecutive days. Longer monitoring periods are

preferred as they will have a higher probability of recording the passing of heavy vehicles.

#### **1.4.2 Connor and Fisher (2006)**

Connor and Fisher provide guidance in using strain gages for the evaluation of out of plane distortion in web gap details. According to their estimates, “90% of all fatigue cracking is the result of out-of-plane distortion or other unanticipated secondary stresses at fatigue sensitive details” (Connor & Fisher, 2006). Field instrumentation is recommended as the preferred tool to properly assess the fatigue life of these details.

It has been previously established that out-of-plane stresses are the driving force behind the formation of the fatigue cracks at web gap details. Moreover, longitudinal bending stresses are not a significant factor as long as the fatigue cracks remain parallel to principal plane of loading. It is recommended that fatigue cracks be arrested prior to the cracks turning perpendicular to the principal plane of loading as traffic loads could significantly advance their growth and potentially lead to unstable brittle fracture. Considering the type of fatigue cracking and its underlying causes, web gap details have been classified as Category C with a CAFT of 10ksi.

Installation of strain gages directly in the web gap region is the recommended approach. Given the likely physical constraints of the web gap, it may be impossible to directly measure the strain at the weld toe. To overcome this limitation, strip-type strain gages capable of providing a strain gradient within the web gap region should be employed. This strain gradient will be used to linearly extrapolate the stresses measured at the gage location to the weld toe. Strip-type gages produced by Measurements Group Inc. Type EA-06-031MF-120 are recommended for

this purpose. It is suggested that the gages not be installed any closer than 3mm from the weld toe. Figure 1.5 illustrates how to obtain weld toe stresses through a linear extrapolation of the measured strains and the strain gradient.

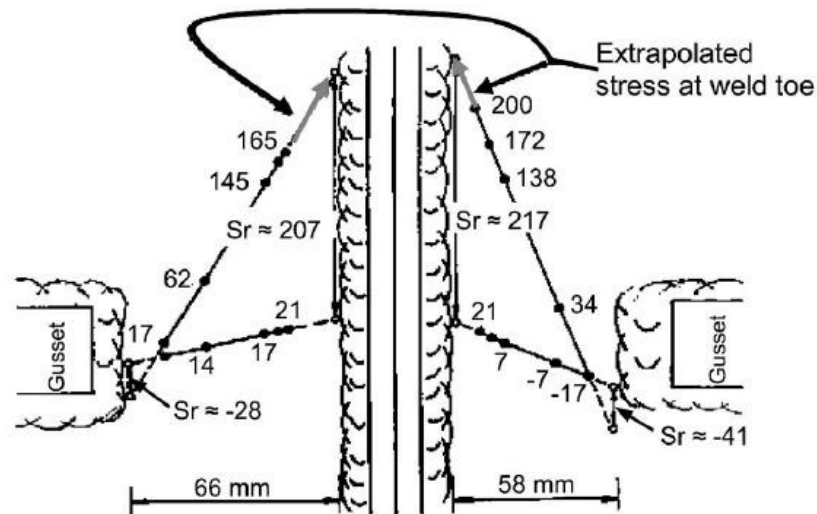


**Figure 1.5** Example of extrapolated stresses (Connor & Fisher, 2006).

In order to capture the full effects of variable traffic, the writers suggest that strain-range histograms should be recorded for a minimum period of two weeks for highways bridges. Longer monitoring periods will likely capture overload or permit vehicles, but given the low frequency of these vehicles they do not cause significant fatigue damage. The Rainflow algorithm and Miner's rule are recommended for cycle counting and effective stress determination respectively. A cutoff value of 0.25CAFT is to be used when determining the effective stress range.

### **1.4.3 Alampalli and Lund (2006)**

Alampalli and Lund present a methodology for fatigue life evaluation and its application to the case study of the Patroon Island Bridge. The AASHTO Guide Specifications for Fatigue Evaluation of Existing Steel Bridges and measured strain data were used to perform a fatigue life analysis of various bridge members. The Patroon Island Bridge is a steel deck truss bridge with floor beams and stringers. It consists of 10 spans carrying Interstate 90 in Albany, NY over the Hudson River with an approximate length of 1,795ft. The bridge was built in 1968 and has an average daily traffic of 70,787 in 1998.

Cracks were detected in the floor beams to deck truss connections at spans 4, 5 and 6 of the Patroon Island Bridge. Strap plates are used to create continuity of the floor beam top flange on both sides of the truss, but they are not directly attached to the truss. In contrast, the web of the floor beams is rigidly attached to the truss with a steel angle. Cracks were detected in this area between the web angle connection and the top flange of the floor beam. These cracks are believed to be caused by large longitudinal deformations of the truss which in turn create out-of-plane bending stresses in the web of the floor beam.

An instrumentation plan was implemented to investigate the remaining fatigue life of various truss members and floor beams in spans 1-3 and 7-10. BDI strain transducers were installed on the bottom flange of beams in positive bending and on the main plates of the truss experiencing tension. Continuous strain data was recorded for 48 hours at a sampling rate of 50 Hz. Strain cycles were obtained from the data using the Rainflow algorithm and parsed into 20 equal-width strain bins.

In order to calculate the effective stress range for a given member using Miner's rule, a lower strain threshold cutoff value must be used. It is well understood

that vehicles weighing less than 20 kips have a very low probability of causing fatigue damage. Instead of simply using a factor of the CAFT as the cutoff value, Alampalli and Lund used the individual strain response of each gage to a 20 kip vehicle. Once the strain gages were installed, traffic was halted and a 37 kip vehicle performed several passes over the bridge. The strain output of each gage was recorded and scaled down by a factor of  $(20/37) = 0.5405$  to obtain the equivalent strain output for a 20 kip vehicle. The result is that each gage location has its own individual strain cutoff value used for calculating the effective stress value.

Remaining fatigue life calculations were done per AASHTO FEESB. The following equation was used:

$$Y_f = \frac{fK \times 10^6}{T_a C (R_s S_r)^3} - a \quad \text{Equation 1.0}$$

Where  $f = 1.0$ ,  $K =$  detail constant found in AASHTO (1990),  $T_a =$  estimated lifetime daily truck traffic,  $C =$  stress cycle per truck passage,  $R_s =$  reliability factor,  $S_r =$  effective stress and  $a =$  present age of the bridge.

The results of the Patroon Island Bridge show that most of the critical details have infinite fatigue life. In other words, the effective stress range caused by the random traffic loads was below the CAFT for that particular detail.

### 1.5 Overview of Approach

Assessing the fatigue life of the Newport Viaduct from measured strains is the goal of this project. The first step was to create a localized finite element model of the Type E diaphragm connection plates. Unlike previous finite element models created, this model used 3D “brick” elements with a higher number of nodes and integration points which will increase the accuracy of the results. This model will be

used to understand the stress distribution surrounding the web gap region prior to conducting the in-service monitoring. The information obtained from the analysis of the finite element models was used to determine the locations and orientation of the strain gages in the field.

In-service field monitoring of the Newport Viaduct was carried out for a period of 23 days. During this time, various measurements were recorded to make possible the subsequent fatigue life analysis of the structure. The Rainflow algorithm was used to determine the number of cycles the structure experiences. Miner's rule was used to determine the effective stress range for the given variable amplitude traffic loading. Per the literature recommendations, several different effective stress cutoff values were used and their results compared.

Given the geometry of the web gap region, it was impossible to directly instrument the weld toe. To overcome this limitation, foil type strain gages were installed directly in web gap while BDI transducers were installed adjacent to the connection plate and the cross frame angles. The data obtained from all the gages was used in conjunction with the localized finite element models to establish an empirical relationship between the stress measured in the web gap region and the weld toe stress. This approach precludes a linear interpolation of the stresses from the web gap to the weld toe.

Lastly, a fatigue life analysis was carried out following AASHTO's Guide Specifications For Fatigue Evaluation of Existing Steel Bridges (1990).

## 1.6 Thesis Outline

This thesis is organized into five chapters. *Chapter 1* provides an introduction to the problem statement, a description of past work done, a review of literature sources and describes the scope of work of the present project.

*Chapter 2* focuses on the finite element models created of the Type E diaphragm connection plates. Two different models were created to understand the behavior of the top web gap and the bottom web gap details. A boundary condition study was carried out to understand the fixity effects, if any, on the stress distribution in the web gap region.

*Chapter 3* describes all aspects of the in-service monitoring of the Newport Viaduct. The different components of the monitoring system are described portrayed and the programming code generated to control the system is discussed. The instrumentation plan used is presented as well as the actual field installation of the gages. Sample plots and tables of the data recorded throughout the length of the in-service monitoring period are also presented herein.

*Chapter 4* details the steps of the fatigue analysis carried out. The bottom web gap finite element model was used in conjunction with the in-service monitoring data to determine the effective stress range at the bottom web gap. Additionally, the number of cycles at the weld toe is extracted from the Rainflow histogram results and lifetime average daily truck traffic (LADTT) values are computed. Mean fatigue life analysis results are presented for varying boundary conditions.

*Chapter 5* presents a summary of the results for the entire project and provides overall conclusions. Current results are discussed I regards to previous work done. Recommendations are given to be implemented during the Newport Viaduct retrofit stage.

## Chapter 2

### FINITE ELEMENT MODELING

#### 2.1 Model Description

In order to assist in the fatigue life analysis of the Newport Viaduct, localized 3D finite element models of the Type E diaphragm connection plates were created. Prior to the field monitoring, these models were used to gain an understanding of the stress distribution near the web gap and this information was used as the basis of the proposed instrumentation plan. Following the field monitoring, these finite element models were used to determine the stresses at the weld toe given that strain gauges could not be directly installed at this location.

The localized finite element models were created in a multi-step process. First, dimensions for the connection plate were obtained from the construction shop drawings used by the contractor Bethlehem Steel Corporation. These dimensions were used to draw 2D surfaces in FEMAP (v.10.1) and later these surfaces were extruded into their final solid 3D form. Given that we are only interested in the stress distribution near the web gap regions, the localized finite element models created are centered about this area exclusively. Next, the localized models were meshed in FEMAP; varying boundary conditions were imposed and a 1.41 kip representative load was applied to the inside of the connection bolt holes. Lastly, the models were converted into an ABAQUS input file and solved.

Some specifics about the finite element models warrant further discussion. After creating solid surfaces and extruding them in 3D, the FEMAP “mesh on Solids”

option was used to create a mesh. The mesh was constructed with a default element size of 0.5, but the “automatic mesh sizing” options were changed to obtain a higher element density in the web gap region. This allowed greater result accuracy in the area of interest, while minimizing computational time by having a coarser mesh in areas other than the web gap. The type of element used throughout the mesh was a 10-noded 3D tetrahedral solid element belonging to the continuum/displacement family of elements known as C3D10 in ABAQUS. This element contains three displacement degrees of freedom, one in each of the X, Y, and Z directions and its output is the 3x3 stress tensor (ABAQUS, 2008). In order to improve the accuracy of the results, reduced integration was avoided altogether and instead full Gaussian Quadrature integration was used throughout the analysis. This resulted in four integration points. Figure 2.1 below illustrates what element C3D10 looks like.

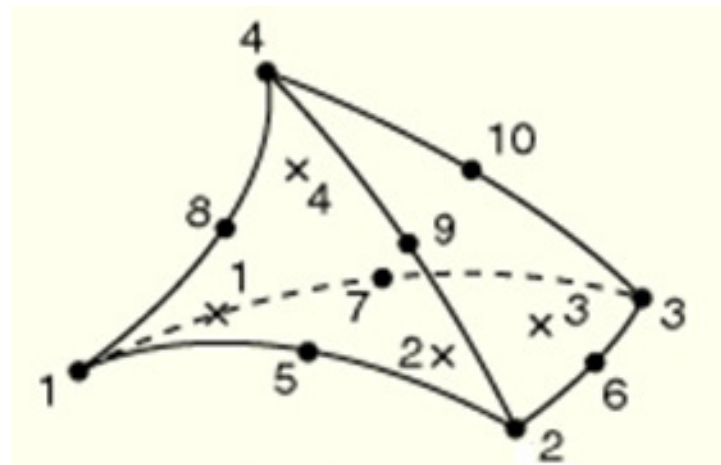


**Figure 2.1 Tetrahedral element with 10 nodes and four integration points. (ABAQUS, 2008)**

In the end, two different localized finite element models were created. This was done because the top and bottom connection plates differ in their bolt hole configuration. While both connections have two  $1\frac{1}{16}$ " bolt holes, their locations are not the same. It is believed that the bolt hole locations may have an effect on the stresses at the weld toe. Geometric dimensions and bolt holes locations were obtained from Bethlehem Steel's shop drawings. Figure 2.2 illustrates the fabrications drawings used for the Type E diaphragms where geometric differences in the top and bottom connection plates can be seen.

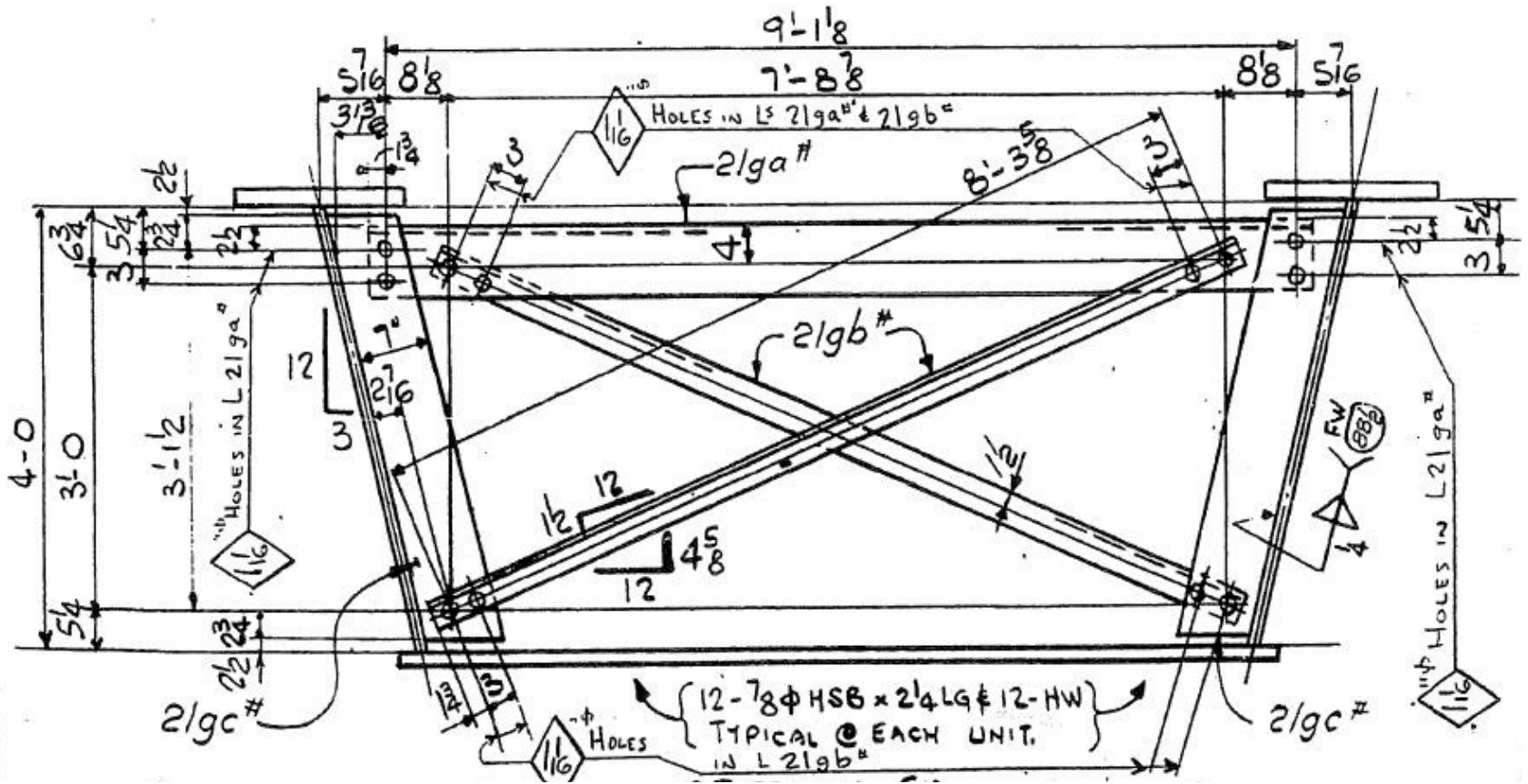
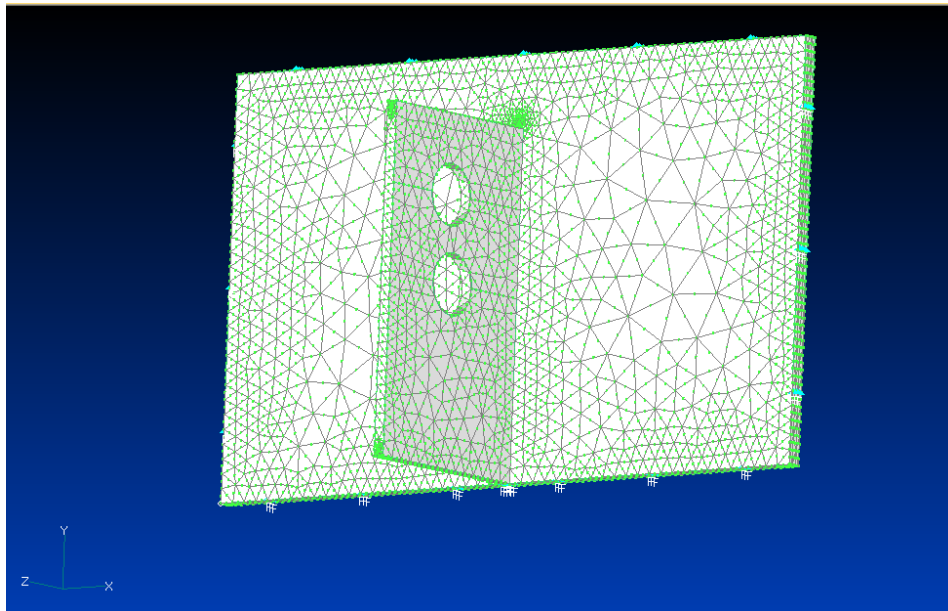


Figure 2.2 Bethlehem Steel fabrication drawings of Type E diaphragms. (Courtesy of DelDOT)

### 2.1.1 Top Connection Model

The top connection model consists of 8,999 solid 10-noded tetrahedral elements and 18,790 nodes. Given the slope of the web, the bolt hole locations are not the same distance from the web. This fact is significant because the resulting line of action from the cross frame loading does not pass through the centroid of the connection and may cause some additional localized bending. This situation will be further investigated in Section 2.2 Boundary Condition Study. Figure 2.3 below illustrates the localized top connection model.



**Figure 2.3 Localized top connection model. Notice higher mesh density in web gap region.**

### 2.1.2 Bottom Connection Model

The bottom connection model consists of 9,092 solid 10-noded tetrahedral elements and 18,999 nodes. Unlike the top connection, the line of action of the cross

frame loading passes through the centroid of the connection. Figure 2.4 below illustrates the bottom connection model.

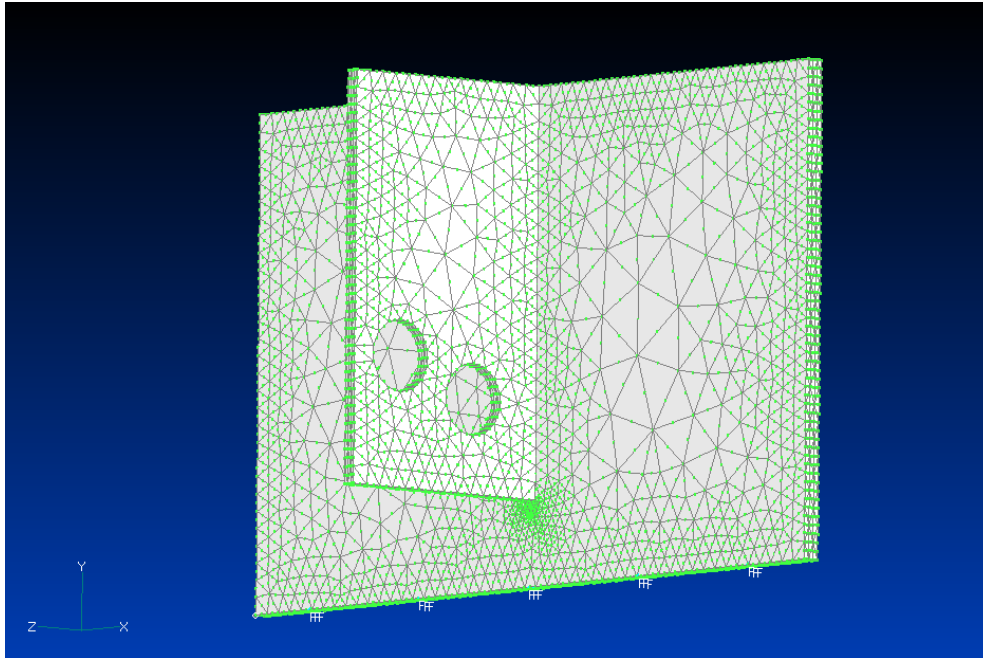


**Figure 2.4** Localized bottom connection model. Notice higher mesh density in web gap region.

### 2.1.3 Model Loading

The loads applied to the localized finite element models were created to replicate the out-of-plane field loadings. It is assumed that the forces originate in the cross frames and are transferred to the connection plate via the bolt holes. These forces are next transferred to the box girder web and in the process create a stress concentration at the weld toe which is believed to be the origin of the fatigue cracks. In an attempt to reproduce this load path, all localized finite element models were loaded on the inside surface of the bolt holes using a distributed load; this load

scenario was created using the FEMAP command “load on surface”. At first, the resultant magnitude of the distributed load was selected as 1.41 kips, simply to gain an understanding of the stress distribution in the web gap region. Figure 2.5 shows the loading conditions for the top connection model.

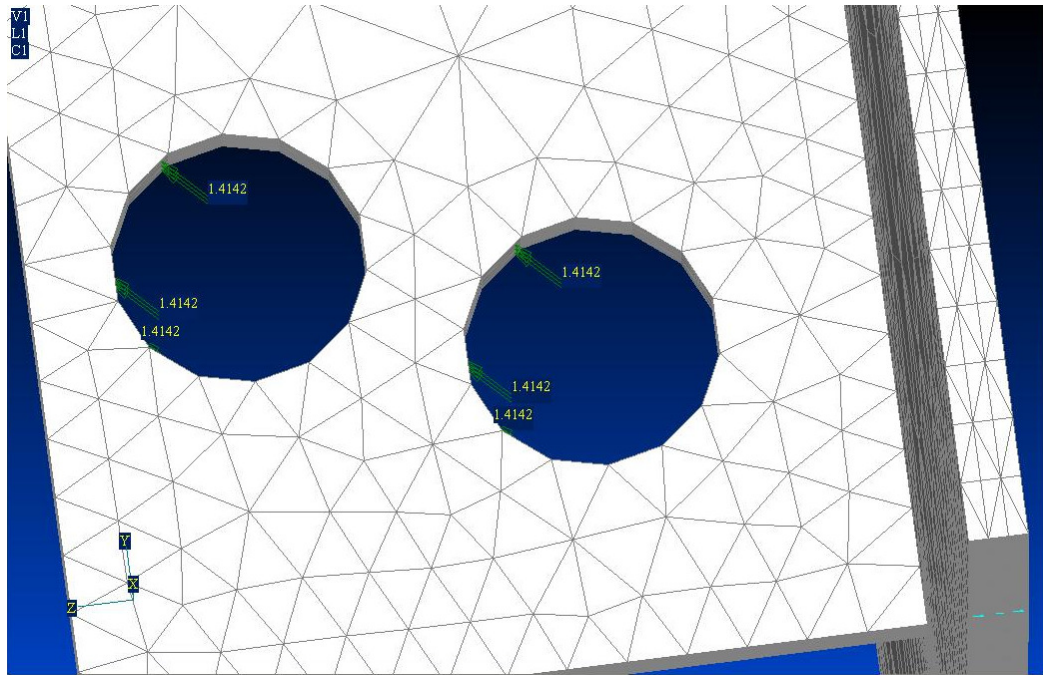


**Figure 2.5 Loading on the inside surface of the bolt holes.**

## **2.2 Boundary Condition Study**

In order to accurately model the stress distribution around the web gap region, it is necessary to propose boundary conditions that reflect the behavior of the structure in the field. These boundary conditions determine the fixity of the localized models in regards to the rest of the structure. However, it is not entirely obvious what the fixity around the edges of the localized models should be. The possibilities range

from fully fixed to completely free edges with the actual field conditions likely being a combination of the above. For this reason, a boundary condition study was carried out to determine the effect of varying the fixity around the localized model edges and its effect on the web gap stress distribution.

In order to capture the full spectrum of possible boundary conditions, three analysis cases were carried out. The first case proposes that all edges of the models are fixed and are not allowed to rotate or displace. The second case proposes that the side edges of the model are to be fixed as well as the top or bottom edge, depending on whether we are analyzing the top or bottom model. Lastly, the third case proposes only the top or bottom edge fixed, depending on the model being analyzed. The idea behind these boundary condition scenarios is to understand the distribution of web gap stresses as a function of the fixity of the edges of the model. Figure 2.6 below illustrates the three boundary condition cases for the top connection model.

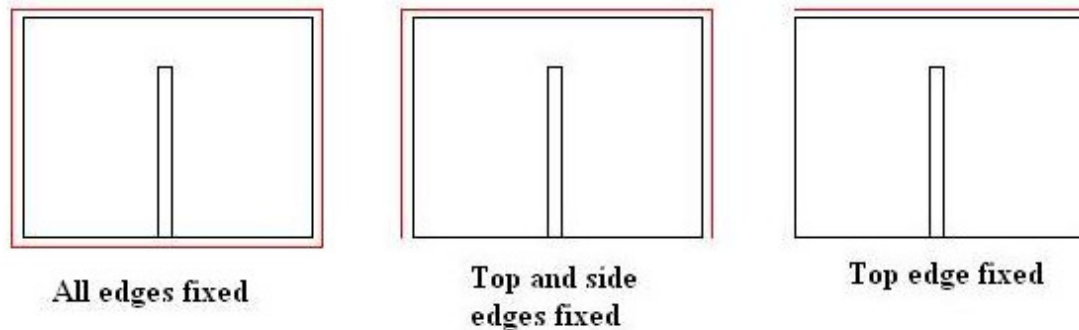


**Figure 2.6** Boundary condition cases for the top connection model.

In addition, the top connection model was subjected to more than just one loading condition scenario. Given that the line of action of the cross frame force does not coincide with the centroid of the top connection, it is desired to understand if this has any effect on the resulting web gap stress distribution and magnitude. For this purpose, the top hole of the connection and the bottom hole of the connection were loaded individually as well as combined. This analysis resulted in three loading conditions scenarios and three boundary conditions scenarios for a total of nine cases for the top connection.

The bottom connection model was subject to three different boundary conditions. Given that the line of action of the cross frame force coincides with the centroid of the bottom connection, it was not necessary to analyze different loading scenarios. The resulting line of action from any individual bolt hole loading will always pass through the centroid of the connection. Table 2.1 on the next page summarizes the different loading and boundary condition scenarios analyzed.

**Table 2.1 Summary of loading and boundary condition cases analyzed**

<b>Model</b>	<b>Loading Conditions</b>	<b>Boundary Conditions</b>
Bottom Connection	Both holes loaded	All edges fixed
		Bottom edge & sides fixed
		Bottom edge fixed
Top Connection	Top hole loaded	All edges fixed
		Top edge & sides fixed
		Top edge fixed
	Bottom hole loaded	All edges fixed
		Top edge & sides fixed
		Top edge fixed
	Both holes loaded	All edges fixed
		Top edge & sides fixed
		Top edge fixed

### **2.3 Finite Element Analysis Results**

The analysis results show the presence of a large stress gradient in the web gap region caused by the cross frame forces. This stress gradient was present in all boundary condition cases and all loading scenarios for the top connection model. Moreover, the results show that the stress concentration due to the cross frame forces is highly localized to the web gap region and does not extend longitudinally along the web of the trapezoidal box girder. Sample stress output plots can be seen in Figures 2.7 -2.9. The results plots from all of the analyses can be found in Appendix A.

The analysis results show that the choice of boundary conditions significantly affects the stress distribution near the web gap for a given loading. For

the bottom connection model, the maximum nodal principal stress at the weld toe decreased as the fixity around the edges was increased. The highest stress was produced when only the bottom edge was fixed, whereas the minimum stress was produced when all edges were fixity. For the top connection model with both holes loaded, the reverse situation occurred. The highest nodal principal stress occurred when all edges were fixed, whereas the lowest occurred when the only the top edge was fixed. This outcome suggests that the top and bottom connection behave quite differently and creating two separate models was warranted. The results of the boundary condition analysis are summarized in Table 2.2.

The different loading scenarios analyzed for the top connection model show very different stress distributions near the web gap. The results show that the maximum principal stresses near the weld toe were significantly higher for the case of only the top hole of the connection being loaded, regardless of the boundary conditions specified. Furthermore, these weld toe stresses were appreciably higher than those obtained from the loading of both holes. Lastly, the lowest stresses near the weld toe were obtained from the load case when only the bottom hole of the connection was loaded. The maximum principal stress results are summarized in Table 2.3

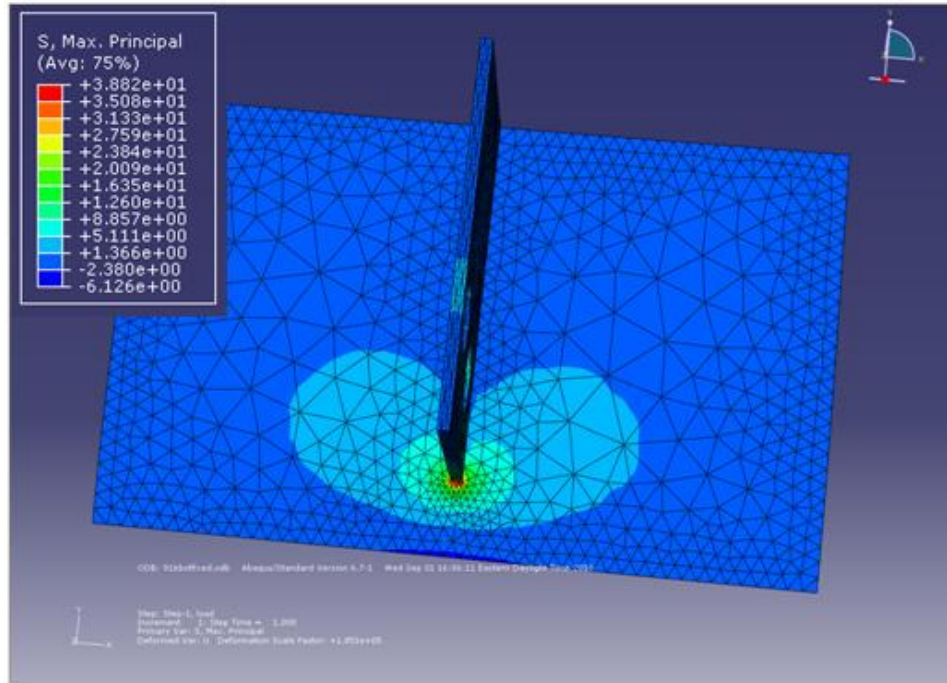


**Figure 2.7** Bottom connection, bottom edge fixed analysis results. Maximum principal stress concentrations are highly localized near web gap region.

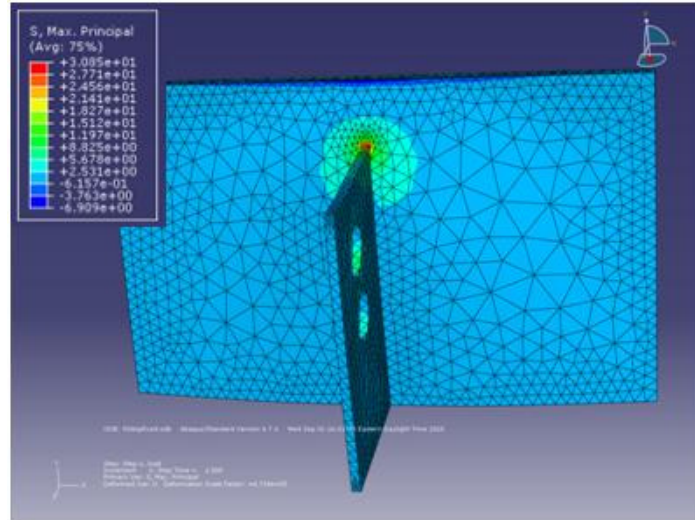


**Figure 2.8** Top connection, top edge fixed. Maximum principal stress concentrations are highly localized near web gap region.

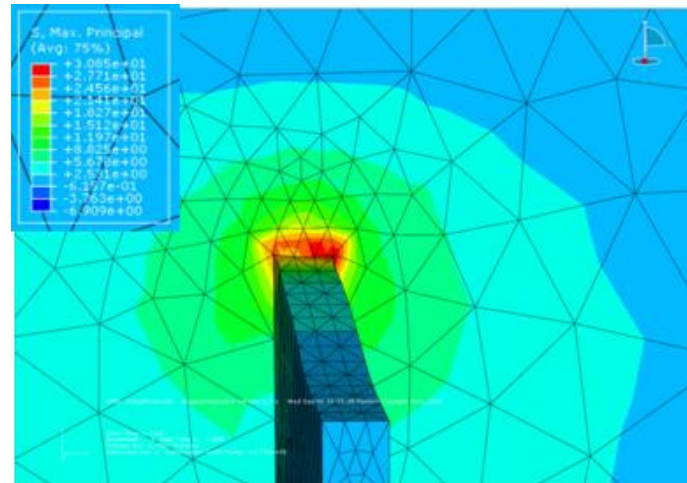


**Figure 2.9** Top connection, top edge fixed zoomed in view. Maximum principal stress gradient becomes extreme near weld toe.

**Table 2.2 Boundary condition study results. All values in ksi.**

<b>Bottom Connection Plate</b>				
	<b>2.82 kip load</b>		<b>Normalized to 1 kip load</b>	
	<b>Min Principal Stress</b>	<b>Max Principal Stress</b>	<b>Min Principal Stress</b>	<b>Max Principal Stress</b>
Bottom Edge Fixed	-6.12	38.82	-2.16	13.73
Bottom and Sides Fixed	-6.79	34.44	-2.40	12.18
All Edges Fixed	-6.87	30.44	-2.43	10.76
<b>Top Connection Plate</b>				
	<b>2.82 kip load</b>		<b>Normalized to 1 kip load</b>	
	<b>Min Principal Stress</b>	<b>Max Principal Stress</b>	<b>Min Principal Stress</b>	<b>Max Principal Stress</b>
Top Edge Fixed	-6.91	30.80	-2.44	10.89
Top and Sides Fixed	-6.90	30.80	-2.44	10.89
All Edges Fixed	-6.23	31.90	-2.20	11.28

Significant conclusions can be drawn from the results of the analysis of the localized finite element models. First, it is evident that the choice of boundary conditions wholly affects the stress distribution near the weld toe. A boundary condition study was carried out to quantify this effect and the results are summarized in Table 2.2. It can be seen that the top and bottom connection models behave quite differently as the boundary conditions are varied. By analyzing the spectrum of possible fixity conditions, the actual field behavior of the structure is captured by some combination of the cases analyzed.

Additionally, Table 2.2 suggests that the bottom connection model is subject to higher stresses than the top connection model. The maximum principal

stress at the weld toe of the bottom connection was higher for all but one of the boundary condition cases analyzed. This situation may be a product of the bolt configuration or perhaps the additional stiffness provided by the concrete deck adjacent to the top connection. Regardless of the cause, higher stresses at the bottom connection would inevitably lead to more fatigue cracks at these locations. The 2007 AECOM inspection report crack list confirms this finding; 75% of the cracks detected occurred at the bottom connection detail. The full crack list from the 2007 inspection can be found in Kucz, 2009.

**Table 2.3 Individual bolt hole loading results for top connection plate.**

<b>Top Connection Plate - Top bolt hole loading</b>				
	<b>1.41 kip load</b>		<b>Normalized to 1 kip load</b>	
	<b>Min Principal Stress</b>	<b>Max Principal Stress</b>	<b>Min Principal Stress</b>	<b>Max Principal Stress</b>
Top Edge Fixed	-2.86	24.59	-2.02	17.39
Top and Sides Fixed	-3.43	21.01	-2.43	14.86
All Edges Fixed	-3.56	18.17	-2.52	12.85
<b>Top Connection Plate - Bottom bolt hole loading</b>				
	<b>1.41 kip load</b>		<b>Normalized to 1 kip load</b>	
	<b>Min Principal Stress</b>	<b>Max Principal Stress</b>	<b>Min Principal Stress</b>	<b>Max Principal Stress</b>
Top Edge Fixed	-4.03	9.67	-2.85	6.84
Top and Sides Fixed	-3.10	11.68	-2.19	8.26
All Edges Fixed	-2.68	13.76	-1.90	9.73

Table 2.3 shows the results of loading individual bolt holes of the top connection plate. It can be seen that singly loading the top hole of the connection creates significantly larger maximum principal stresses at the weld toe than singly loading the bottom hole.

## **Chapter 3**

### **IN-SERVICE MONITORING**

#### **3.1 Overview**

In-order to assist in the fatigue life analysis of the Newport Viaduct, in-service monitoring of the exterior (west) girder in spans 9-11 southbound direction was carried out. On November 17, 2010 a monitoring system consisting of 8 strain gages, data logger and power source was installed in locations of interest near one Type E diaphragm. Strains were recorded for a period of 23 days and the monitoring system was retrieved on December 16, 2010. DeIDOT personnel and equipment were employed to gain access to the inside of the trapezoidal box girder and provide support as needed. Given the confined space nature of the box girders, proper training and permitting was carried out in conjunction with the Environmental Health and Safety Office at the University of Delaware.

The in-service monitoring of the Newport Viaduct had several essential goals. Continuous in-service monitoring of the structure will directly measure the magnitude and number of loading cycles caused by variable traffic. The data obtained during the monitoring period will be used in conjunction with the finite element models discussed in Chapter 2 to determine the effective stress at the weld toe of the Type E diaphragm connection. The use of finite element models was warranted because direct measurement of the stresses at the weld toe was not possible given the physical constraints of the Type E diaphragm connection plates. A comprehensive

description of the instrumentation plan, equipment used, test setup and data obtained is presented in the next sections.

### **3.2 Monitoring System**

The monitoring system used for this project consisted of three main components: data logger, strain gages and power source. Additionally, a wireless cellular modem was used to remotely operate the monitoring system.

#### **3.2.1 Datalogger**

The data logger is the central part of the monitoring system responsible for processing the voltage differential output from the strain gages and recording the values for future use. The data logger chosen for this purpose was the Campbell Scientific CR5000 Measurement and Control System. The CR5000 data logger makes measurements up to 5,000 samples/second with 16-bit resolution and features 20 differential input channels measuring voltages up to  $\pm 5V$ . The CR5000 data logger can be powered by a 12V external battery, the internal 7 amp-hour lead acid battery or by using the 120VAC adapter; thus, allowing great flexibility when selecting a power source. The measured data can be stored in either the internal 1MB EEPROM memory or a PCMCIA card for convenient transfer and manipulation (Campbell Scientific, 2006). Moreover, the CR5000 supports peripherals such as a wireless modem which can be used to remotely operate the data logger as well as download the recorded data. Given the length of time that the monitoring system was out in the field and the physical access limitations of the inside of the Newport Viaduct box girders, this remote operation capability was fully utilized. Lastly, the CR5000 offers extreme programming flexibility in regards to data recording and analysis. It can carry out

computations on the data as it is measured, thus simplifying the subsequent data analysis for the user. Figure 3.1 illustrates the CR5000 data logger.



**Figure 3.1 CR5000 data logger with 120VAC adapter and PCMCIA data card.**

### 3.2.2 Strain Gages

Two different types of strain gages were used as part of the monitoring system. Two electrical resistive foil type strain gages were installed directly in the web gap region and 6 BDI ST-350 strain transducers were used at the other locations. Three different methods were used to attach the gages to the locations of interest. Foil gages were welded in place directly in the web gap region. Foil gages possess the disadvantage of being somewhat fragile and require a lengthy installation process, but their use was imperative to capture stresses in the web gap region. Even though BDI

strain transducers have an effective length of 3 inches, their overall length is in excess of 4 inches and simply could not be installed in the 2.5 inch web gap region. On the other hand, BDI strain transducers were easily clamped to other locations such as the cross frame angles. In locations where clamping was not possible, steel tabs were threaded through the gages and bonded to the steel surface using adhesive. The adhesive used was Loctite 410 together with its accelerant Loctite 7452. The steel surface was grinded to remove all paint to ensure proper adherence of the steel tabs. Upon completion of the in-service monitoring, the areas where the steel tabs were mounted were repainted to prevent rusting.

The BDI strain transducers are individually calibrated to an accuracy of  $\pm 2\%$  per NIST standards and possess a strain range of approximately  $\pm 4,000 \mu\epsilon$  (Bridge Diagnostics, 2006). Each BDI strain transducer has an identification number with a corresponding gage calibration factor supplied by the manufacturer. These gage factors were obtained and incorporated into the programming of the data logger for each individual gage to ensure accuracy of the results. Each BDI strain transducer possesses 350 Ohm resistance and has 4 leadwires which are wired directly into the data logger. The transducers were powered with a 5V excitation. These electrical properties were used to determine the amount of power each transducer and the entire monitoring system consume. Figure 3.2 on the next page illustrates a typical BDI Strain Transducer ST-350.

The foil gages used were manufactured by Micro-Measurements and are part of the General Purpose Sensor – Linear Pattern family. The foil gages used in the monitoring system are fully encapsulated K-alloy gages with high-endurance leadwires. The overall gage length is 0.720 inches with a matrix length of 0.92 inches

(Micro-Measurements, 2010). Each foil gage has 3 lead wires, which become 4 wires after they are wired through the Terminal Input Modules. The resistance of the foil gages is 350 Ohms and they have a strain range error of  $\pm 1.5\%$ . Figure 3.3 below illustrates a typical foil gage.



**Figure 3.2** BDI strain transducer ST-350.

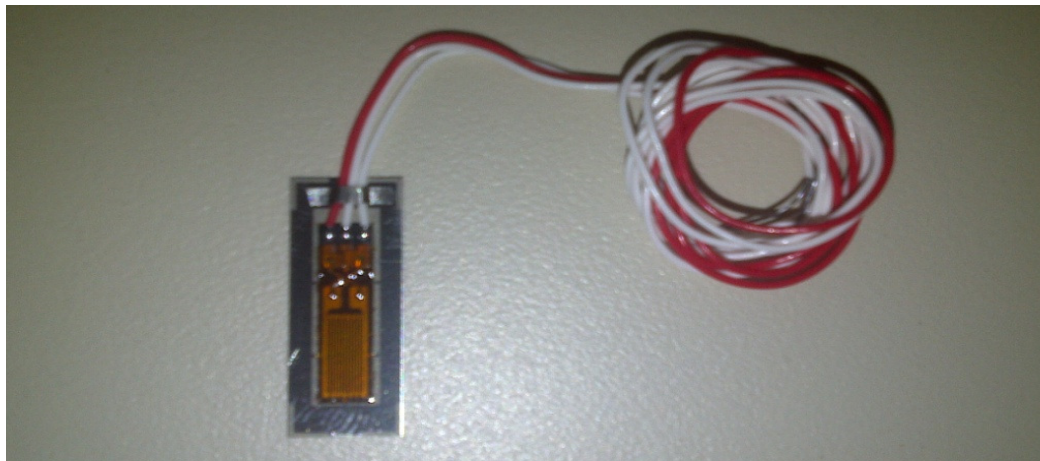


**Figure 3.3** Quarter bridge Micro-Measurements foil gage

The BDI strain transducers consist of a full Wheatstone bridge while the foil gages consist of a quarter Wheatstone bridge. As such, it becomes necessary to complete the resistance bridge in order for the foil gages to properly function. Terminal Input Modules (TIMs) manufactured by Campbell Scientific were used for this purpose. TIMs “provide completion resistors for resistive bridge measurements” (Campbell Scientific, 2009) and attach directly to the data logger. Figure 3.4 shows a typical Terminal Input Module.



**Figure 3.4** Campbell Scientific Terminal Input Modules to be used with foil gages/

### **3.2.3 Cellular Modem**

The RavenXTV CDMA Sierra Wireless Cellular Modem was used as a part of the monitoring system in order to remotely operate the CR5000 data logger. The Raven cellular modem runs on the Verizon Wireless network and is specifically

designed to function with Campbell Scientific dataloggers. A 10-digit Mobile Directory Number (MDN) was setup through Verizon Wireless and it was used to establish a dynamic IP address. This IP address was used to establish a connection via the internet to the cellular modem and allow remote operation of the monitoring system. The RavenXTV runs on an 800MHz cellular band and consumes 120mA 12Vdc during transmission (Campbell Scientific, 2009). In order to maximize wireless signal reception inside the box girder of the Newport Viaduct, a PN 18285 1 dB Omni Directional Antenna was used with the RavenXTV. Even though the monitoring system was installed inside a steel box girder with a composite concrete deck, wireless signal strength was not an issue. Figure 3.5 below illustrates the RavenXTV and antenna.



**Figure 3.5 Raven XTV cellular modem and Omni Directional Antenna**

### **3.3 CR500 Datalogger Programming**

#### **3.3.1 RTDAQ Software**

Programming of the CR5000 datalogger was done using the Real Time Data Acquisition (RTDAQ) software package. RTDAQ is “Campbell Scientific’s Datalogger Support Software targeted for industrial and other high-speed data acquisitions” (Campbell Scientific, 2008). RTDAQ’s Program Generator module was used to create a comprehensive control program for the CR5000 datalogger without having to employ advanced programming techniques. The Program Generator module within RTDAQ is an easy to use graphical user interface capable of generating a control program in Basic code. As part of the control program, it was necessary to specify the data logger scan rate, the type and quantity of sensors used, the corresponding gage factors and the desired output tables. Beyond programming, RTDAQ was used to remotely operate the datalogger and manipulate recorded data files. Figure 3.6 on the next page is a screenshot of the Program Generator module within RTDAQ.

#### **3.3.2 Measurements**

The sampling rate of the datalogger was set at 100Hz to ensure the capture of dynamic events. However, this fast sampling rate would generate an enormous amount of data if its output were recorded for all 8 strain gages. For this reason, the output data tables generated had significantly larger time intervals. Nonetheless, raw data at 100Hz was recorded for several hours in order to gain insight into the global behavior of the Newport Viaduct. Raw data measurements at 100 Hz were used to create extreme event “snapshots”. Each snapshot shows the strain history of all strain gages for a given extreme event such as a heavy truck passing, usually no more than a

few seconds long. Albeit brief, these snapshots provide a clear picture of the structure's response to a severe loading. All recorded data tables and raw data snapshots can be found in Section 3.4 Field Measurements.

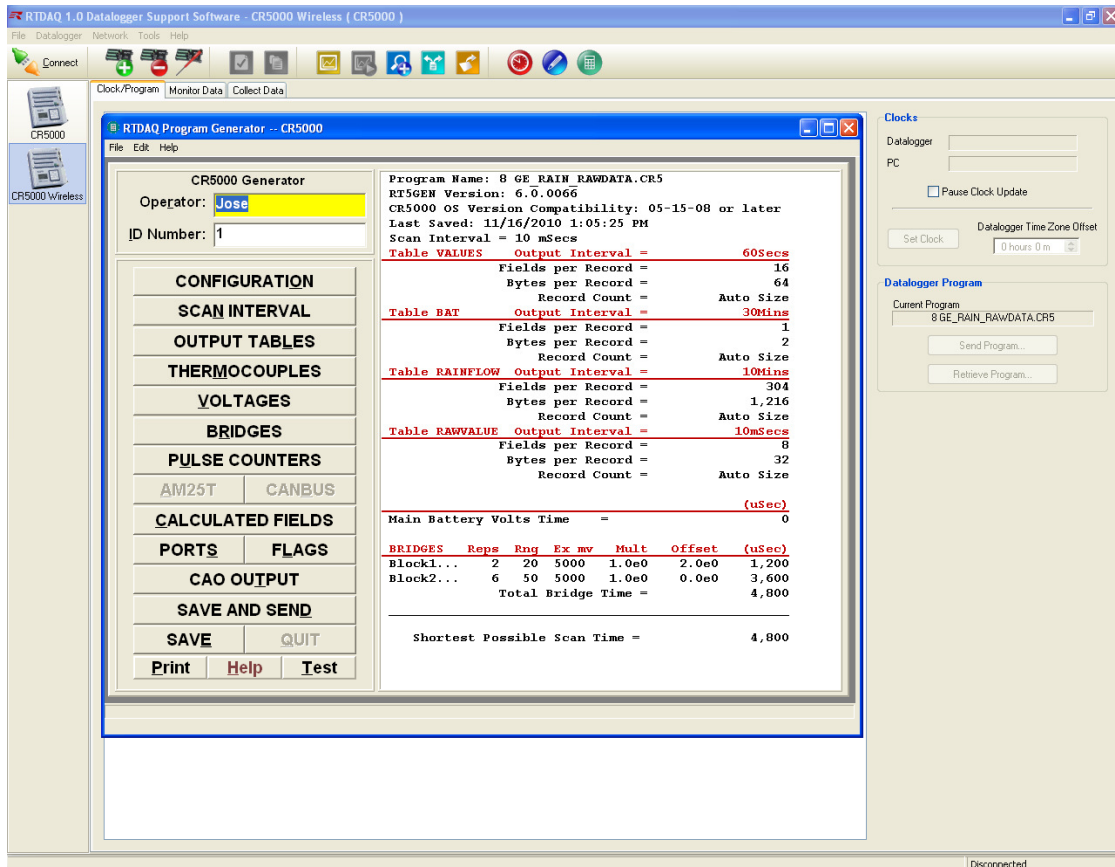


**Figure 3.6** Program Generator module within RTDAQ. A summary of the output tables is shown.

The CR5000 datalogger was programmed to produce several different output tables with different time intervals. First, stress range histograms were produced using the Rainflow algorithm for cycle counting. This algorithm “detects the

peaks and valleys of the strain history and determines the cycle counts for all levels of measured stress ranges” (Alampalli, 2006). The Rainflow algorithm is pre-programmed into RTDAQ, thus it was relatively simple to select it as an output table option. The Rainflow histogram output table used the 100Hz scan rate, but its entries were spaced at 10 minute intervals. The downside of having the datalogger process the raw data and generate the Rainflow histogram automatically is the inability to view the raw data. To address this setback, the next output table was programmed to capture the maximum and minimum strain values recorded by each strain gage every 60 seconds. While significantly lower than the 100Hz scan rate, this output table will show extreme events at the Newport Viaduct on 60 second intervals. Data from this output table such as the maximum strain in the cross frames will be used as the loading condition of the localized finite element models described in Chapter 2. Lastly, an output table recording battery voltage on 30 minute intervals was created. This table was used to survey the power source of the monitoring system and assure sufficient voltage was available throughout the monitoring period. This table was of particular importance, as the CR5000 datalogger will automatically shut down if its power source drops below 11V. Through the use of the cellular modem, all output tables as well as real-time data could be remotely viewed throughout the monitoring period.

### **3.3.3 Power Consumption Estimates**

Given the confined space nature of the test location, the entire monitoring system was powered by a pair of heavy duty 12V batteries. Each battery had a stated capacity of 100Ah at 12V, but given their old age and lack of charging cycles their actual capacity was taken as 50Ah. As such, it was of paramount importance to accurately estimate the monitoring system current requirements, to ensure the batteries

capacity was not be exceeded. Following a conservative approach, the CR5000 internal 7Ah battery was not considered as a current source for the monitoring system and simply deemed reserve capacity. Figure 3.7 below shows one of the batteries used.



**Figure 3.7** One of two 12V batteries used to power the monitoring system.

Manufacturer supplied electrical properties were used to estimate the current drain of the various monitoring system components. At 5V and 350 $\Omega$  resistance, each strain gage consumes 15mA of current each hour. The datalogger current consumption is a function of its scan rate. Campbell Scientific provides current drain estimates for the CR5000 datalogger for scan rates of 1Hz and 5MHz.

Interpolating in between this range, it was determined the CR5000 datalogger consumes 8.5mA of current at a sampling rate of 100Hz (Campbell Scientific, 2006).

The RavenXTV modem consumes 50mA in dormant mode and 120mA while transmitting/receiving (Campbell Scientific, 2009). Since the RavenXTV modem was exclusively used to allow remote operations of the datalogger, it was not necessary to supply it with power 24 hours a day. In order to preserve the batteries, the cellular modem was only powered during 2 hours each day. Thus, remote operation of the CR5000 datalogger was only possible during this daily 2 hour window.

Establishing this daily power-up window for the Raven XTV allowed its daily current drain to be limited to only 240mA instead of 1,340mA. This reduction of the daily current needed by the RavenXTV allowed for a longer monitoring period to be carried out given the limited capacity of the batteries. Table 3.1 on the next page summarizes the estimated current drain of the monitoring system.

Selectively supplying power to the RavenXTV for 2 hours each day was accomplished by using the SW-12 power out port in the CR5000 datalogger. The SW-12 port can be switched on/off per instructions in the program being executed. However, this programming feature was beyond the capabilities of the Program Generator module in RTDAQ. To overcome this limitation, the code produced in the Program Generator module was edited in the CRBasic Editor, another module within RTDAQ, to include control commands for the SW-12 port.

It was desired for the SW-12 port to turn on at 11:00am and turn off at 1:00pm, thus only providing power to the modem during this period. This was accomplished by using the “iftime” command which references the internal clock in the datalogger. The logic used is described herein. If the datalogger time was the 11<sup>th</sup>

hour of a 24 hour cycle, then the SW-12 port was switched on. Likewise, if the datalogger time was the 13<sup>th</sup> hour of a 24 hour cycle, the SW-12 port was switched off. This instruction was embedded within the larger control program which was constantly running during the monitoring period. The actual code used to power the RavenXTV is shown below while the entire programming code can be found in Appendix B.

```
If IfTime(11,24,4) Then SW12(1)      'Turn the SW12 switch on at the 11th hour
If IfTime(13,24,4) Then SW12(0)      'Turn the SW12 switch off at the 13th hour
```

**Table 3.1 Current consumption estimates for the monitoring system.**

<b>Component</b>	<b>Hourly current consumption (mA)</b>	<b>Daily current consumption (mA)</b>
8 Strain Gauges @15mA	120	2,880
Datalogger @ 100Hz	8.5	204
RavenXTV modem (2 hours/day)	120	240
Total daily current consumption		3,324
Estimated battery capacity		100,000 mAh
Estimated maximum length of field monitoring		30.1 days

Assuming a conservative capacity of 50Ah for each battery, the power consumption estimates suggest sufficient current is available to power the monitoring system for at least 30 days. Moreover, 7Ah are available in the internal battery of the datalogger which could provide additional current if needed.

As previously stated, in-service monitoring of the Newport Viaduct was carried out for 23 days and during this time no power issues were encountered. In fact, the monitoring system was retrieved after 29 days of being deployed and it was still running off the 12V batteries, albeit with a significant drop in the voltage of the batteries.

### **3.4 Instrumentation Plan**

The instrumentation plan was designed with several goals in mind. First, it was desired to record stresses at the web gap region. Weldable foil gages were chosen for this purpose and were installed in both the top web gap region and the bottom web gap region. Next, it was desired to measure cross frame forces. To accomplish this, BDI transducers were clamped to the bolted angle legs of the Type E diaphragm. Next, it was desired to determine the number of loading cycles the bridge was subject to. For this purpose, BDI transducers were installed with adhesive on the bottom flange and mid-web of the box girder. Lastly, BDI transducers were installed adjacent to connection plate at the beginning of the web gap. These gages were used to gain information of the stress distribution surrounding the web gap region and compare it to the results of the finite element models. Figure 3.8 below illustrates the instrumentation plan.

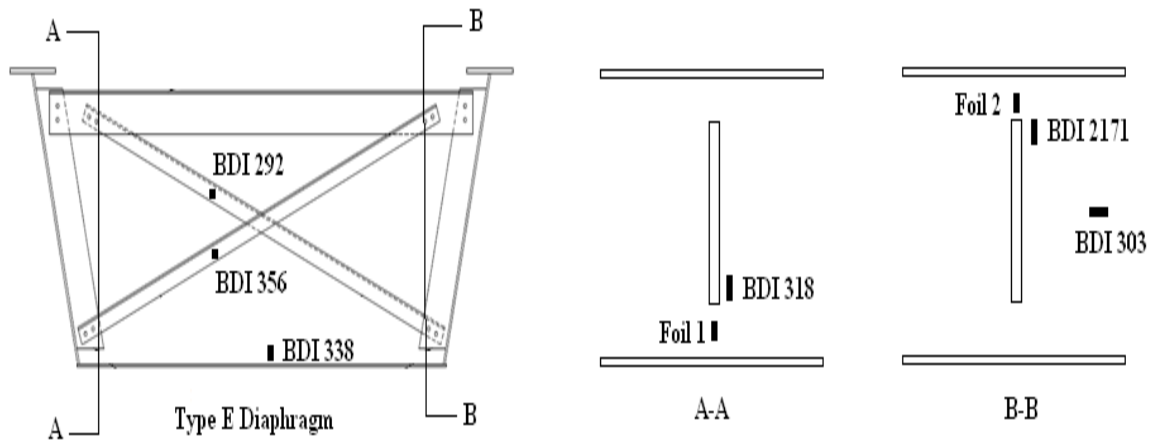


**Figure 3.8 Strain gage instrumentation plan.**

### 3.5 Field Setup

The monitoring system was installed at the Newport Viaduct on the morning of November 17, 2010. Specifically, it was installed on the second type E diaphragm from Pier 10, within the southbound exterior box girder. Assuming most trucks travel in the right lane, this location was chosen with the intent of primarily capturing their effects. Emphasis was placed on recording the effects of truck traffic since research suggests that a vehicle weighing less than 20 kips “has a very low probability of causing fatigue damage” (Alampalli, 2006). A DelDOT bucket truck was used to enter the box girder through the access hole adjacent to pier 10 above Ayre Street. Figure 3.9 on the next page shows the location where the monitoring system was installed on the bridge plans.

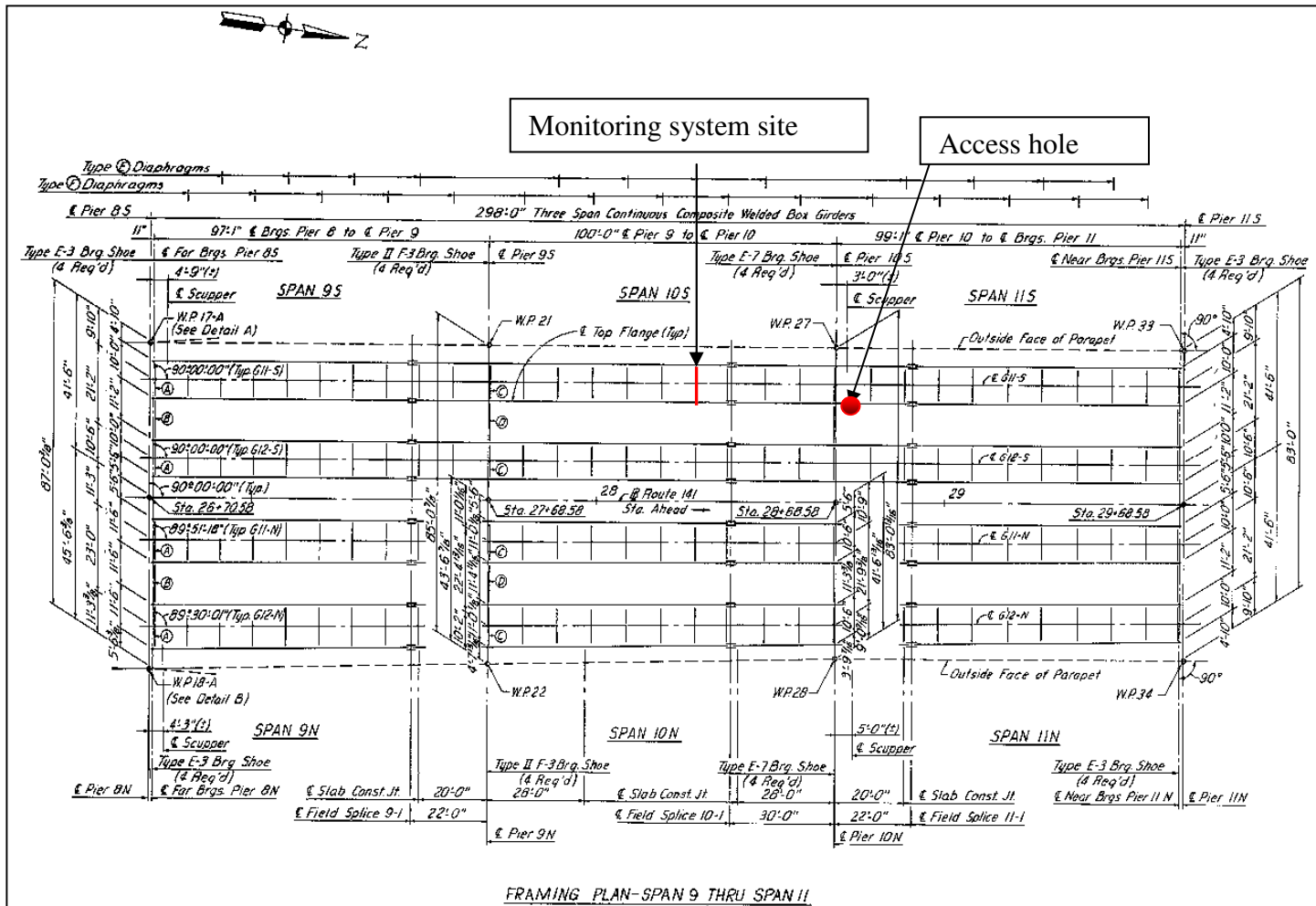
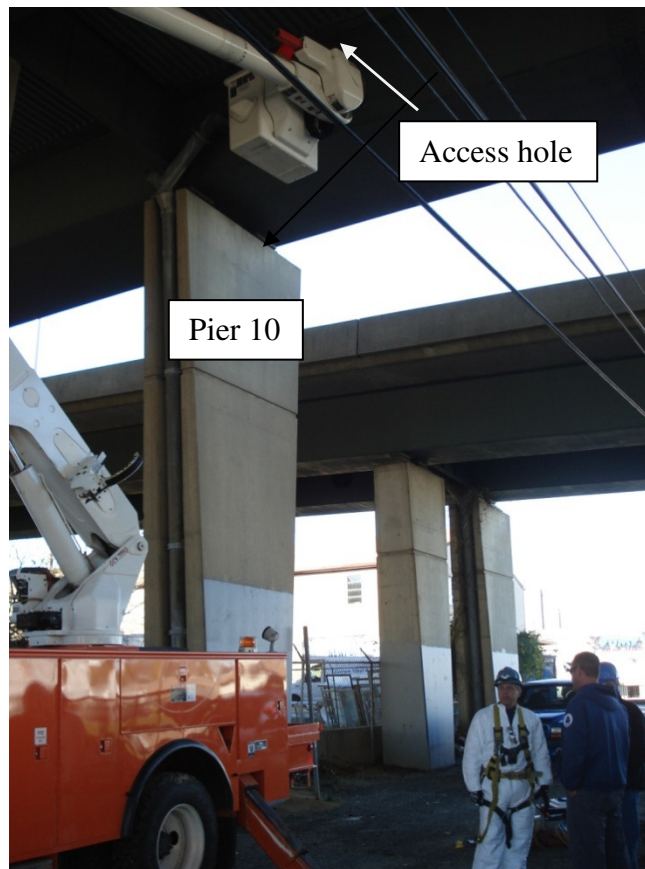
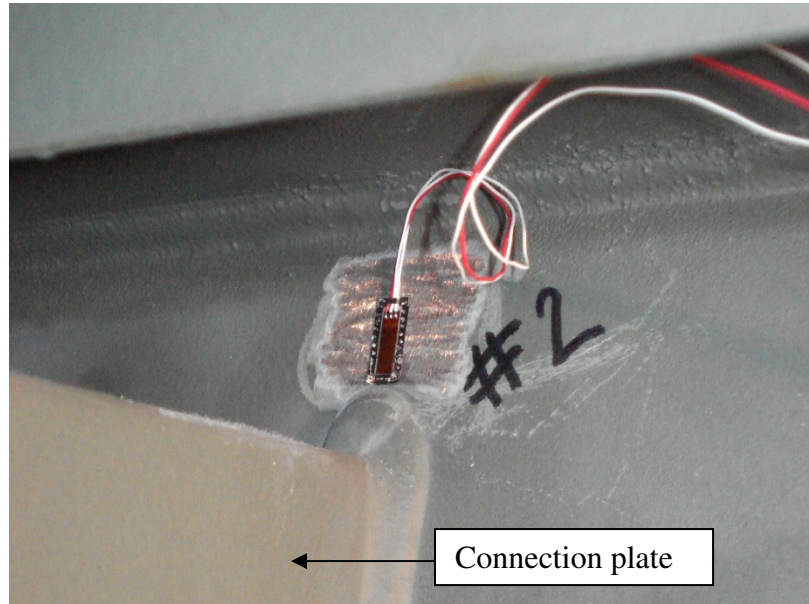


Figure 3.9 Location where monitoring system was installed. (DelDOT, 1972)



**Figure 3.10 DelDOT bucket truck used to reach access hole above Ayre Street**

The access hole above Ayre Street was located approximately 40 feet above the street. As such, it became necessary to utilize a bucket truck to access it and to use safety harnesses for fall protection. Figure 3.10 shows the location of the access adjacent to pier 10. Figures 3.11-3.13 in the following pages illustrate the installation of the strain gages near the Type E diaphragms.



**Figure 3.11** Installation of foil gage #2 on top web gap region.



**Figure 3.12** BDI transducers clamped to the bolted legs of cross frame angles.

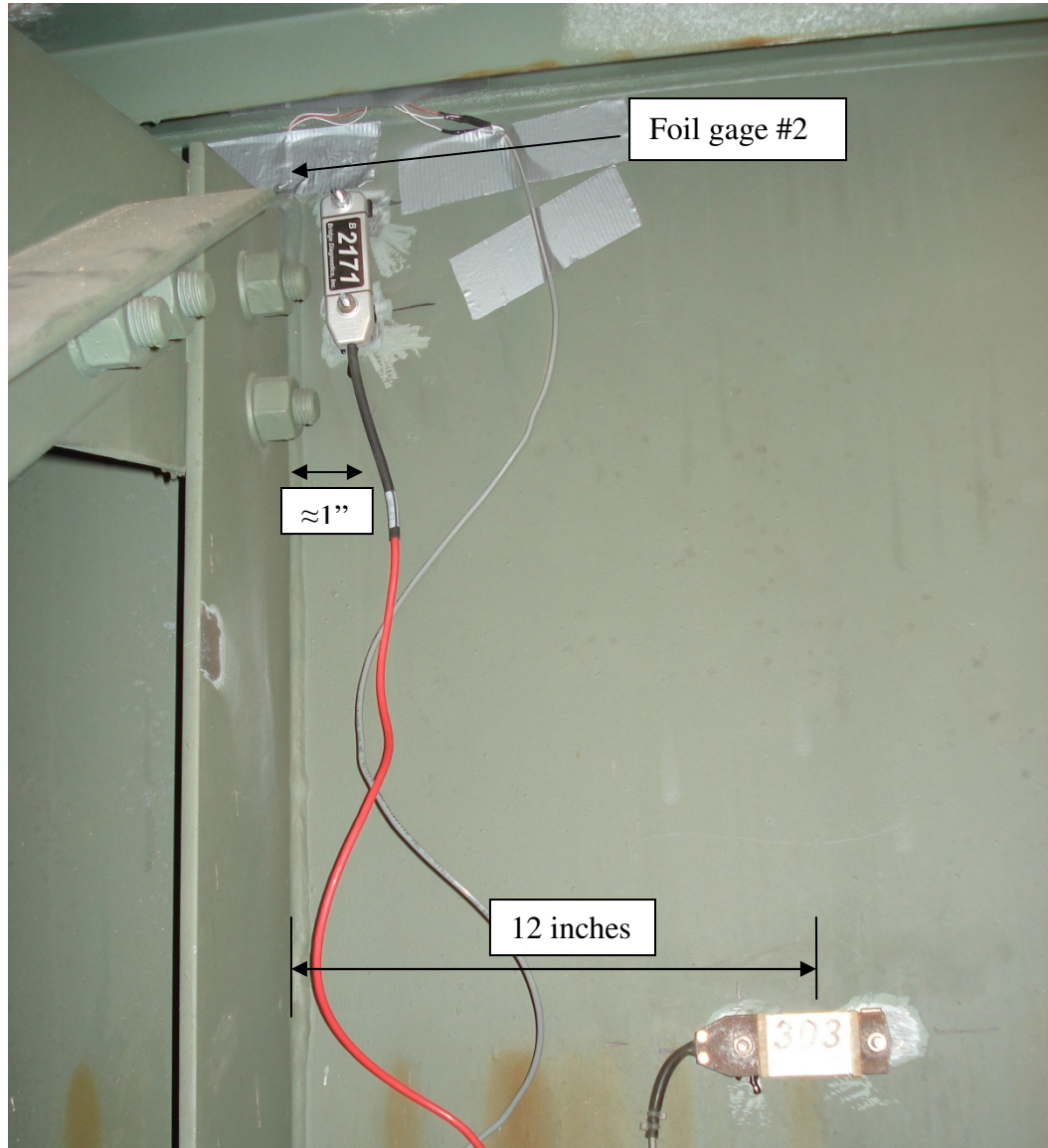


**Figure 3.13 View of strain transducers and foil gage after installation.**

To accelerate the field installation process, each strain gage was connected to its appropriate port on the CR5000 prior to field deployment. This was a very important step, as each gage has a unique identification number which was included in the monitoring program and the output tables.

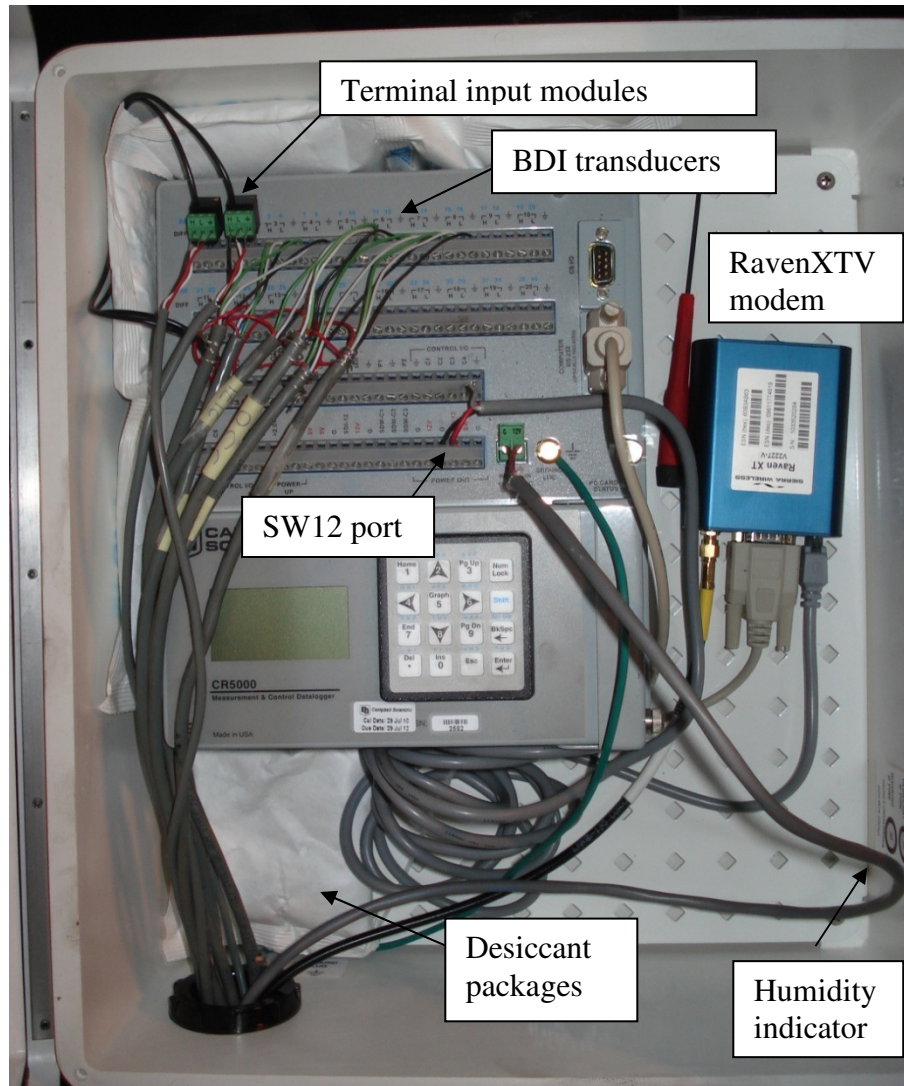


**Figure 3.14 Final wiring of monitoring system.**

The CR5000 datalogger and Raven XTV modem were stored inside a Campbell Scientific junction box throughout the duration of the field monitoring. In order to prevent moisture damage to the electronic equipment, DESI PAK® desiccant packages were placed inside the junction box. Upon retrieval, the inside of the

junction box showed no signs of moisture, as evidenced by the humidity indicator.

Figure 3.14 shows the final wiring of the monitoring system on site.

### **3.6 Data Recorded**

Several different output tables were created from the data recorded during the in service monitoring of the Newport Viaduct. The Rainflow algorithm was used to parse the strain gage measurements into specific bins as a function of its amplitude. Originally, it was desired for all strain gage measurements to be parsed into the same number of bins, however due to unexpected programming issues this was not the case. The amplitude measured by the foil gages was parsed into 38 bins while the amplitude of the BDI transducers was parsed into 20 bins. Thus, the histograms for the foil gages and BDI transducers have different bin ranges and do not lend themselves for comparison. The median value of the each bin was used to calculate the corresponding stress. Table 3.2 summarizes the histogram results of the BDI transducers and Table 3.3 summarizes the results for the foil gages.

Additionally, maximum/minimum values were recorded for each of the strain gages in one minute intervals. Datalogger measurements were taken 100 times per second for each gage, but only the maximum/minimum values every minute were recorded. These measurements will provide a per minute time history of extreme events for the duration of the in service monitoring.

Lastly, it was desired to obtain some data at the full 100Hz to understand the global behavior of the bridge under variable traffic. However, recording data at 100Hz for 8 strain gages generates data files of tremendous size and it was not feasible to store them in the PCMCIA card. For this reason, raw data at 100Hz was recorded on the morning of December 14<sup>th</sup> between approximately 5:00 am and 7:30am. These

raw data files were used to create data snapshots that show the instantaneous output of all strain gages for a given extreme event and can be found in section 3.6.1. Sample histograms and plots are shown in this chapter; complete data output histograms and plots can be found in Appendix C.

**Table 3.2 Rainflow histogram results for BDI transducers**

<b>Bin</b>	<b>Range (<math>\mu\epsilon</math>)</b>	<b><math>\sigma</math> (ksi)</b>	<b>BDI 303 MW</b>	<b>BDI 292 XF #1</b>	<b>BDI 2171 TWG</b>	<b>BDI 338 BF</b>	<b>BDI 356 XF#2</b>	<b>BDI 318 BWG</b>
1	5-9.5	0.21	18333	553042	919105	22012	187501	1332271
2	9.5-19	0.41	0	125691	377071	10579	36252	599404
3	19-28.5	0.69	0	16470	45253	2129	5294	75955
4	28.5-38	0.96	0	4818	13882	224	2027	21017
5	38-47.5	1.24	0	2088	6325	1	637	9617
6	47.5-57	1.52	0	1348	3088	0	84	4478
7	57-66.5	1.79	0	665	2070	0	2	2504
8	66.5-76	2.07	0	239	1508	0	0	1531
9	76-85.5	2.34	0	73	841	0	0	987
10	85.5-95	2.62	0	6	448	0	0	805
11	95-104.5	2.89	0	1	333	0	0	555
12	104.5-114	3.17	0	0	232	0	0	331
13	114-123.5	3.44	0	0	156	0	0	200
14	123.5-133	3.72	0	0	80	0	0	130
15	133-142.5	3.99	0	0	41	0	0	71
16	142.5-152	4.27	0	0	10	0	0	28
17	152-161.5	4.55	0	0	1	0	0	10
18	161.5-171	4.82	0	0	2	1	0	4
19	171-180.5	5.10	0	0	1	0	0	1
20	180.5-190	5.37	0	0	0	0	0	0

As expected, the lower bins have greater number of cycle counts than the higher bins. Figures 3.15-3.16 show a sample Rainflow histogram plot for gage BDI 318.

**Table 3.3 Rainflow histogram results for foil gages**

<b>Bin</b>	<b><math>\mu\epsilon</math></b>	<b><math>\sigma</math> (ksi)</b>	<b>FG #1 Bottom</b>	<b>FG #2 Top</b>
2	5-10	0.22	1242117	19389
3	10-15	0.36	202413	3315
4	15-20	0.51	59385	1075
5	20-25	0.65	22449	344
6	25-30	0.80	9701	117
7	30-35	0.94	4790	30
8	35-40	1.09	2558	8
9	40-45	1.23	1436	0
10	45-50	1.38	805	0
11	50-55	1.52	406	0
12	55-60	1.67	239	0
13	60-65	1.81	134	0
14	65-70	1.96	79	0
15	70-75	2.10	49	0
16	75-80	2.25	35	0
17	80-85	2.39	22	0
18	85-90	2.54	13	0
19	90-95	2.68	10	0
20	95-100	2.83	9	0
21	100-105	2.97	7	0
22	105-110	3.12	3	0
23	110-115	3.26	3	0
24	115-120	3.41	1	0
25	120-125	3.55	3	0
26	125-130	3.70	0	0
27	130-135	3.84	2	0
28	135-140	3.99	0	0
29	140-145	4.13	3	0
30	145-150	4.28	1	0
31	150-155	4.42	0	0
32	155-160	4.57	0	0
33	160-165	4.71	0	0
34	165-170	4.86	0	0
35	170-175	5.00	0	0
36	175-180	5.15	0	0
37	180-185	5.29	0	0
38	185-190	5.44	2	0

Foil gage #1 was installed in the bottom web gap connection detail, while foil gage #2 was installed in the top web gap region. Table 3.3 shows the Rainflow cycle counting results for the strain gages located in the web gap region. It can be seen that foil gage #1 experiences a significantly larger number of events and higher stress magnitudes than foil gage #2. As suggested by the finite element analyses and confirmed by the in-service monitoring, the bottom web gap region experiences higher magnitude stresses and higher number of cycles. Figures 3.15 and 3.16 show the Rainflow histogram for foil gage #1.

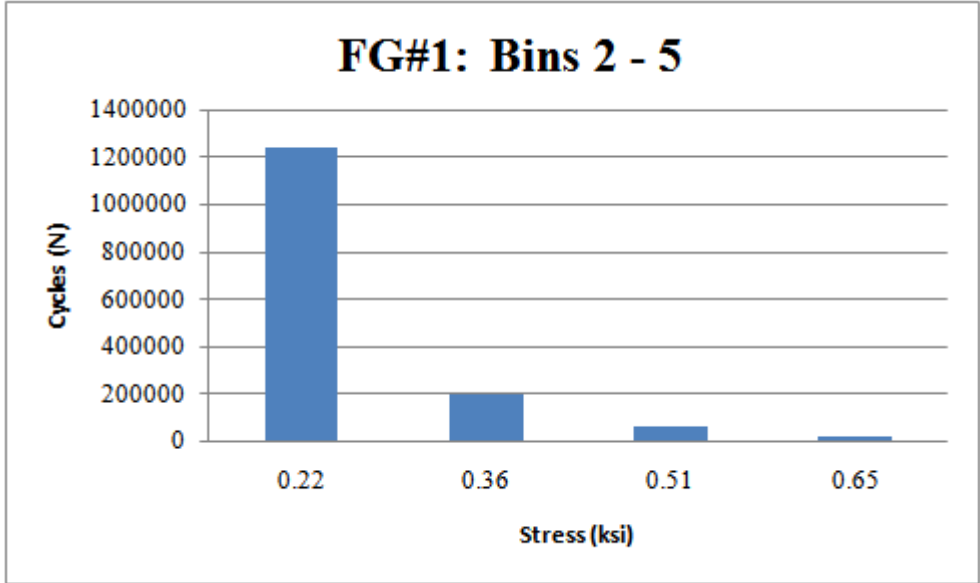


**Figure 3.15 Rainflow histogram for foil gage #1, bins 2-5.**

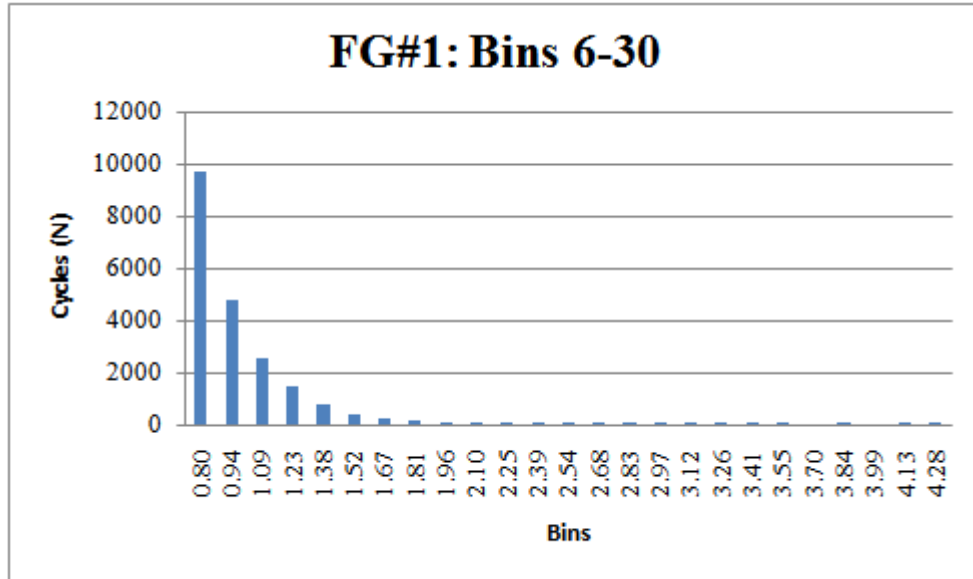


**Figure 3.16 Rainflow histogram for foil gage #1, bins 6-30.**

The minimum/maximum values were recorded in one minute intervals for each gage. All gages were “zeroed” at the beginning of the in-service monitoring period. However, the recorded results still did not necessarily exhibit a zero mean as expected. This can be attributed to vehicles being on the bridge as the gages were zeroed or due to thermal variation effects. For this reason, the absolute average of all recordings was taken for each gage and subtracted from every value. This procedure ensured that the maximum/minimum readings for every gage have a zero mean. Time history responses of gages which had this “de-meaning” done are referred to as “averaged” throughout this paper. Figure 3.17 below shows the averaged minimum/maximum graph for gage BDI 2171.

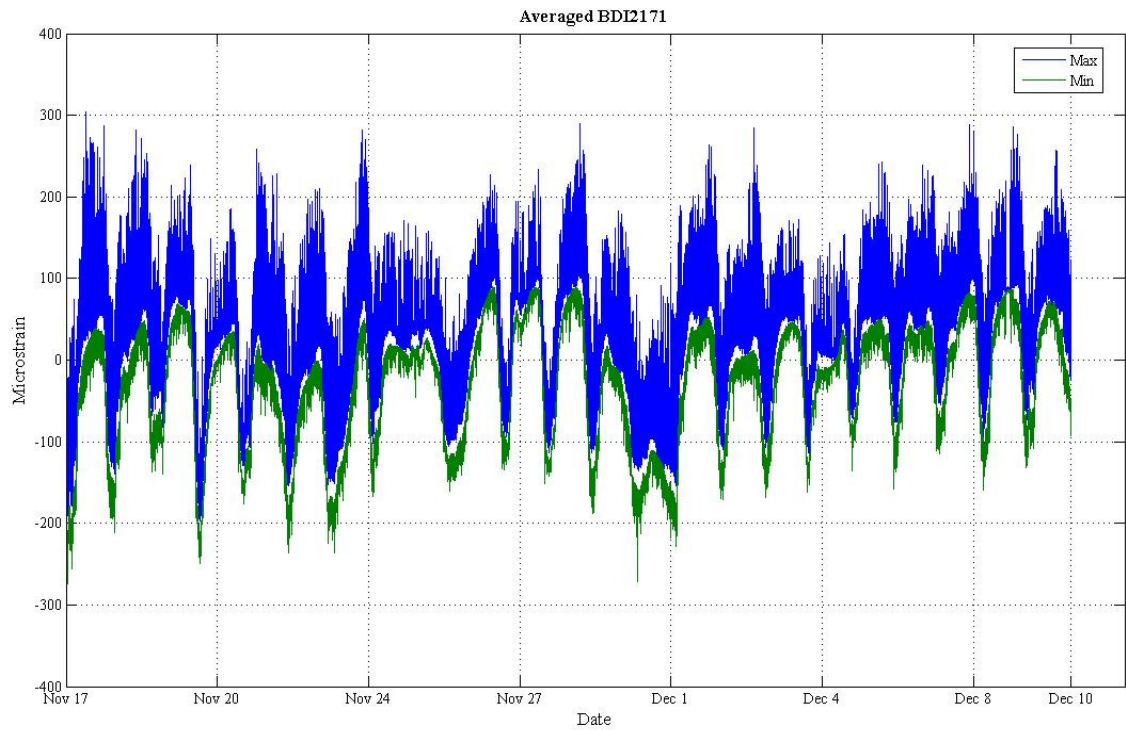


**Figure 3.17 Averaged maximum/minimum recordings for BDI 2171**

With the intent of capturing the effects of rush hour traffic, on the morning of December 14<sup>th</sup> between approximately 5:00am and 7:30am, data values were recorded at 100Hz for each gage. The recorded values show the instantaneous response of the bridge for traffic loading during this period of time. Figure 3.18 on the next page shows the recorded values at 100 Hz for gage BDI 2171.

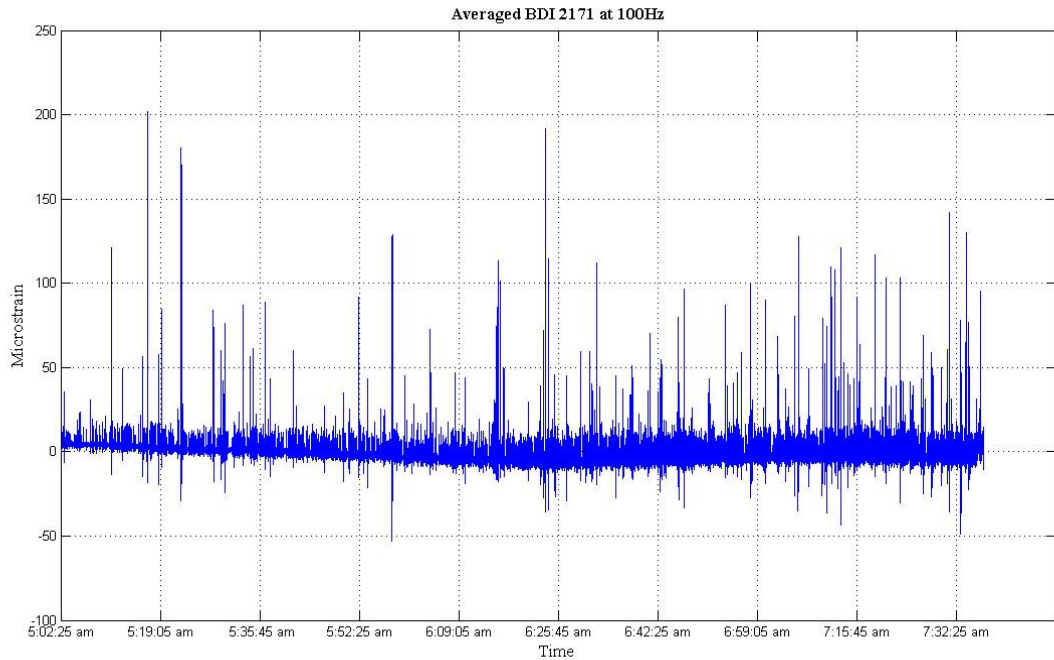


**Figure 3.18** Averaged data recorded for BDI 2171 at 100Hz.

### 3.6.1 Extreme Event Snapshots

The values recorded at 100Hz were used to understand the global behavior of the bridge. A time interval was defined surrounding a peak event for cross frame gage BDI 356. This time interval was chosen between the times of 5:10:45.660 am and 5:11:05.660 am on December 14, 2010. Figures 3.19 -3.22 show the output of every gage over this time interval.

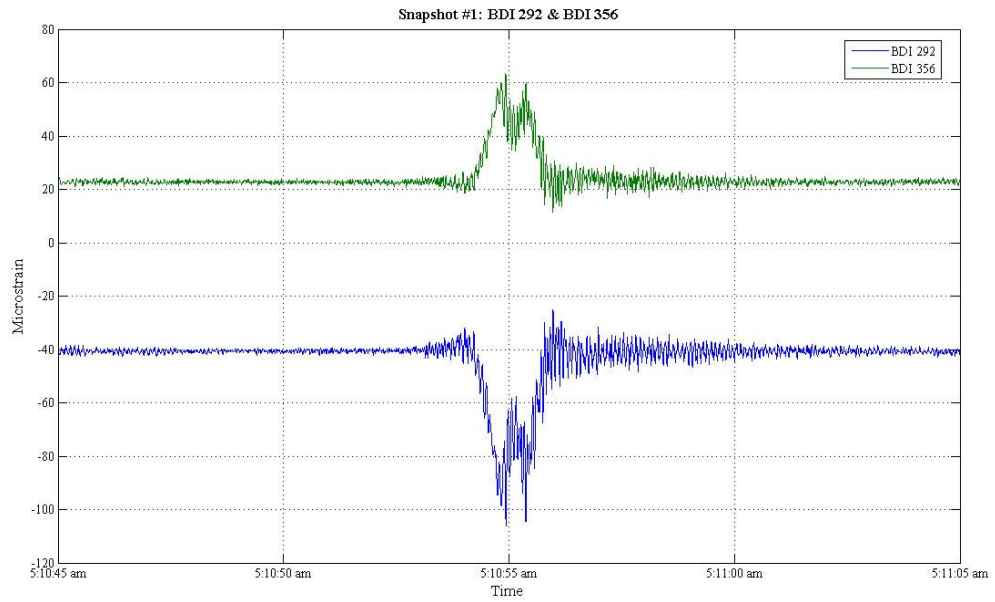


**Figure 3.19 Snapshot event #1 cross frame gages.**

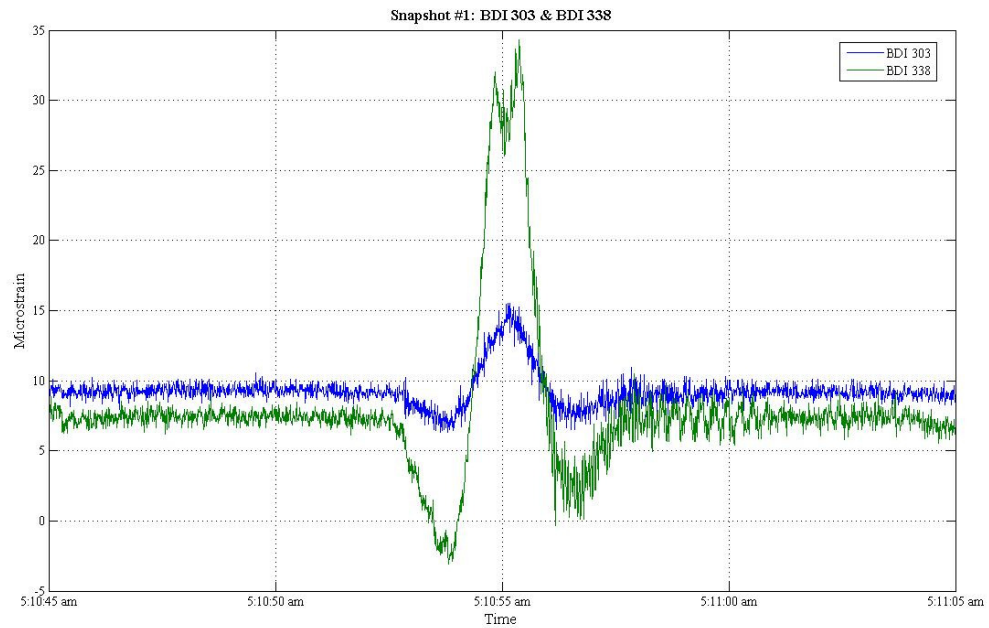


**Figure 3.20 Snapshot event #1 mid-web and bottom flange gages.**

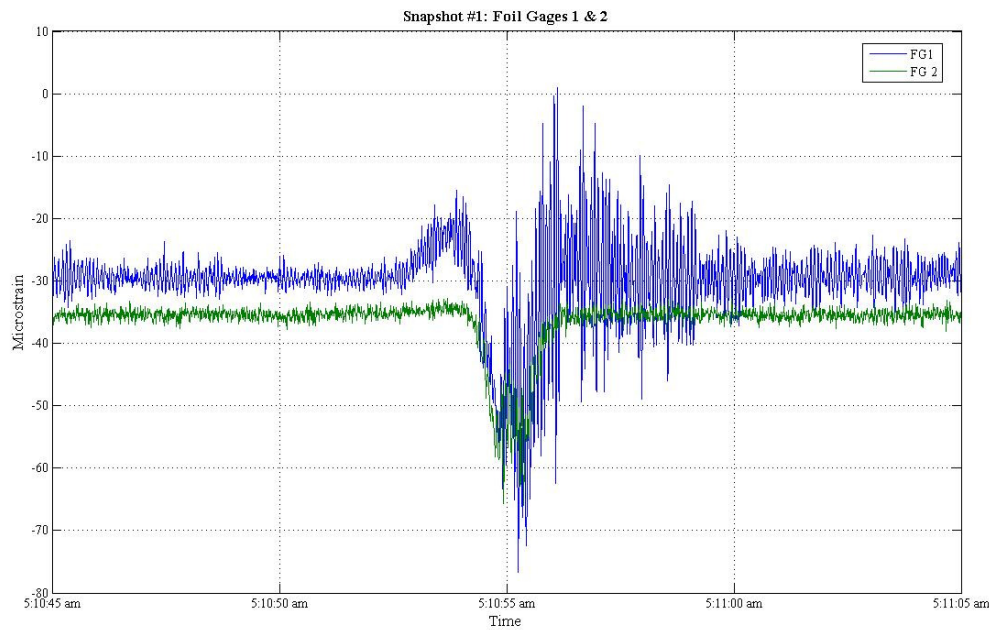


**Figure 3.21 Snapshot event #1 web gap foil gages #1 & #2.**

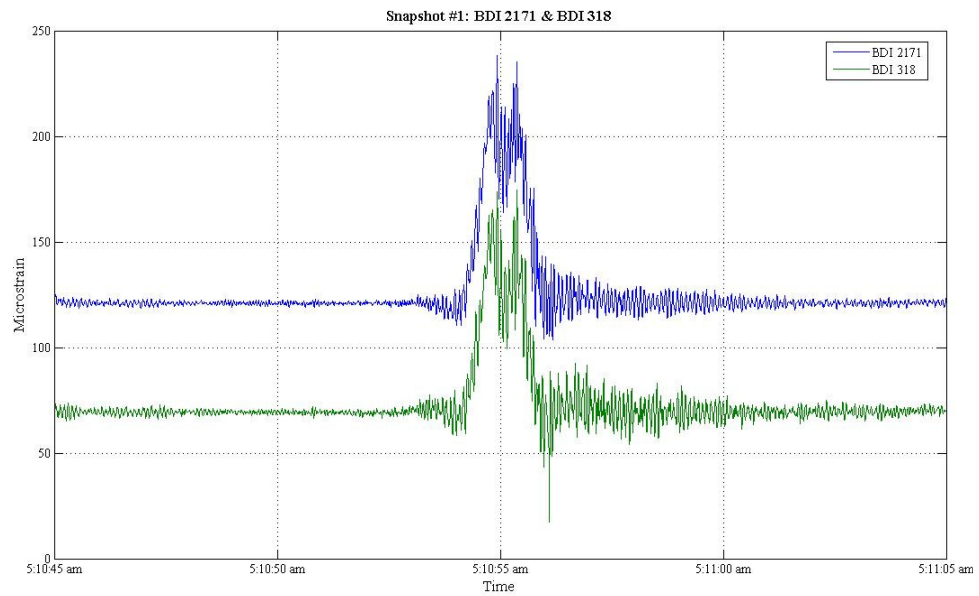


**Figure 3.22 Snapshot event #1 BDI gages adjacent to connection plate.**

Using a peak interval for the bottom flange gage BDI 338, a second snapshot event was created for comparison purposes. The time interval selected for this snapshot event was between 5:16:45am and 5:17:05 am on December 14, 2010. Figures 3.23 – 3.26 show the output of every gage over this time interval.

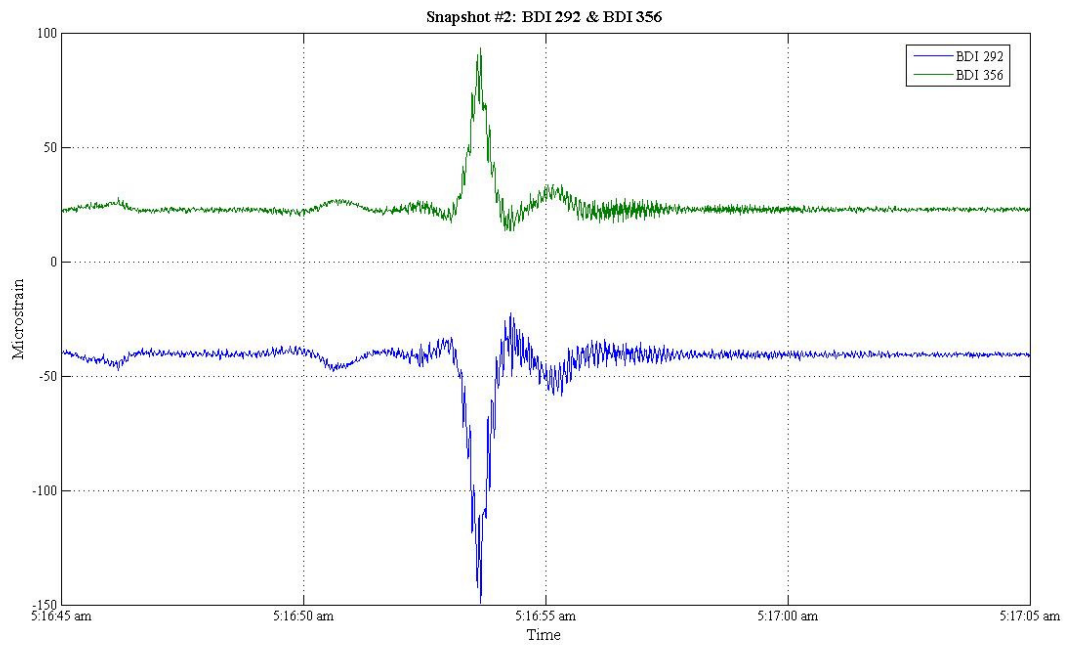


**Figure 3.23 Snapshot event #2 cross frame gages.**

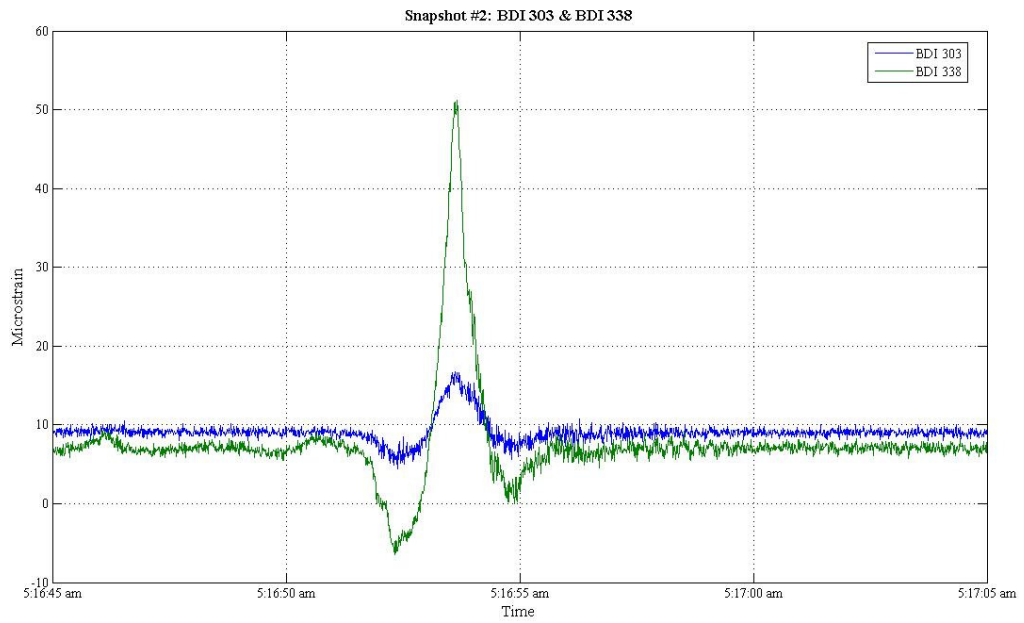


**Figure 3.24** Snapshot event #2 mid-web and bottom flange gages.

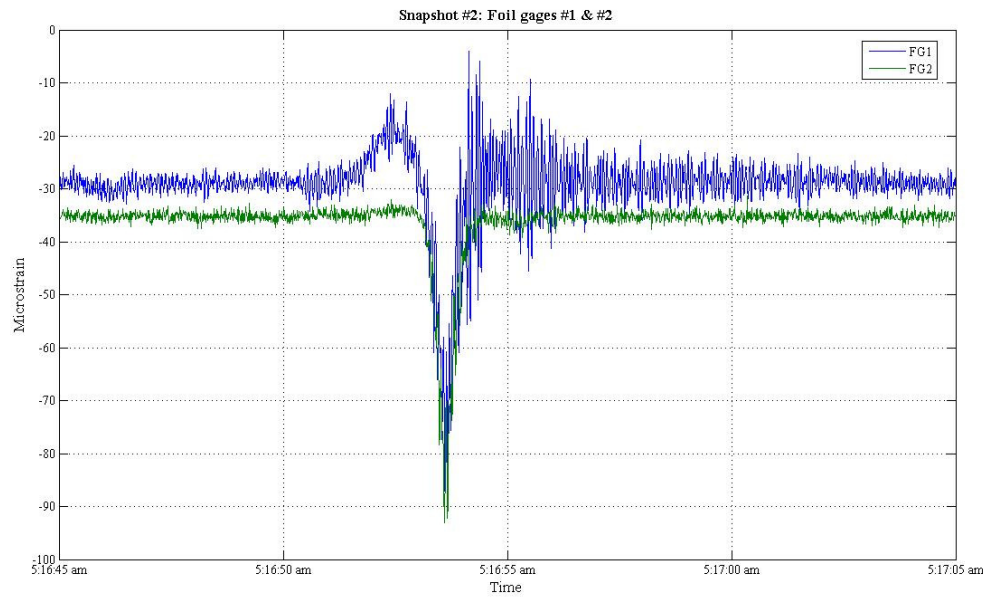


**Figure 3.25** Snapshot event #2 web gap foil gages #1 & #2.

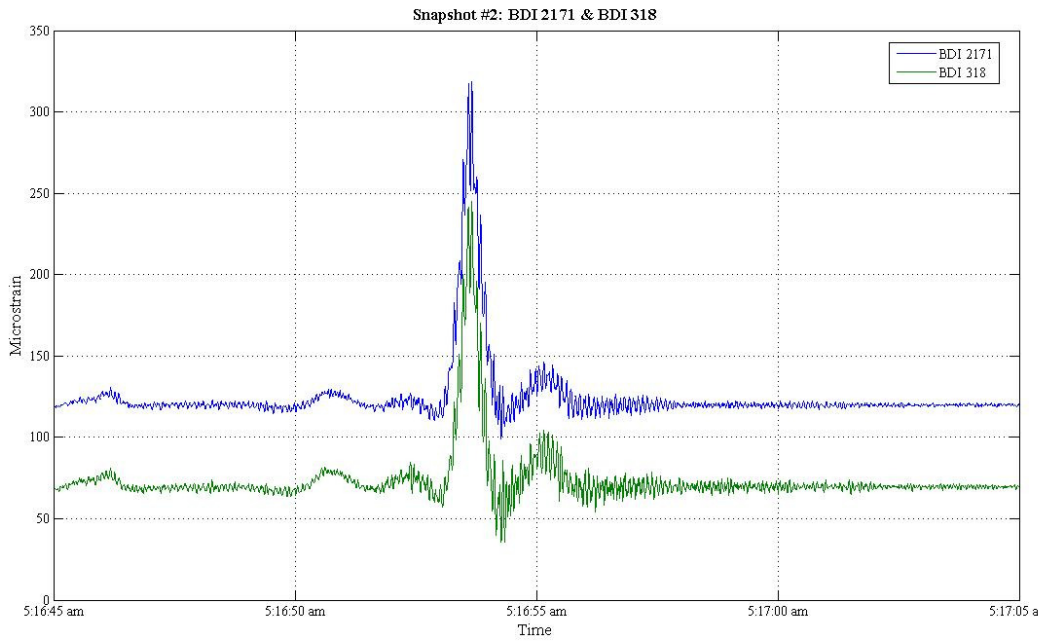


**Figure 3.26 Snapshot event #2 BDI gages adjacent to connection plate.**

## Chapter 4

### FATIGUE LIFE ANALYSIS

#### 4.1 Methodology

The procedures outlined in AASHTO's Guide Specification for Fatigue Evaluation of Existing Steel Bridges (FEESB) (1990) were used to analyze the fatigue life of the web gap connection details at the Type E diaphragms. It has been previously established that the bottom connection detail exhibits larger stresses and number of cycles than the top connection detail. As such, it is expected that the bottom connection detail will have a shorter fatigue life. The fatigue life analysis presented herein will focus on the bottom connection since it is expected to control the overall fatigue life of the structure.

For the purpose of this analysis, remaining mean life was chosen as it "is the best possible estimate of the actual remaining life" (AASHTO, 1990). The remaining mean fatigue life of a detail is given by:

$$Y_f = \frac{fK \times 10^6}{T_a C (R_s S_r)^3} - a \quad \text{Equation 4.1}$$

Where  $f=2.0$  for mean life,  $K=12$  for a Category C detail,  $T_a$  is the lifetime average daily truck traffic,  $C$  is the number of cycles per truck passage,  $R_s=1$  is a reliability factor associated with the calculation of stress range,  $S_r$  is the effective stress range and  $a$  is the current age of the structure in years. According to FEESB, for continuous span girders with a length greater than 40 feet,  $C=1$ . The values for the effective stress

( $S_r$ ) and lifetime average daily truck traffic ( $T_a$ ) are determined in the following sections.

#### **4.2 Stress at Weld Toe**

Determining the effective stress at the detail of interest is a central requirement for carrying out a fatigue life analysis. For the case of the Type E diaphragm connection plates, the physical limitations of the web gap region made it impossible to directly measure the stress at the weld toe. To overcome this drawback, the bottom connection localized finite element model was used to determine the stress at the weld toe. Miner's rule was subsequently applied to determine the effective stress range used as an input for Equation 4.1

A numerical relationship was established between the stress at the foil gage location and the corresponding maximum stress at the weld toe. To accomplish this, the foil gage location from the in-service monitoring was superimposed on the bottom connection finite element model. The finite element model was loaded using a 1.4142 kip load perpendicular to the girder web which corresponded to an out of plane force transferred from the cross frames. Longitudinal stresses from the bending of the entire girder were not included in the analysis as it has been well established that their effects are "much smaller than the local out of plane bending stresses" (Connor & Fisher, 2006). Next, the model was analyzed with varying boundary conditions and the nodal output was recorded at the superimposed gage location and corresponding maximum at the weld toe. Once the stresses at the gage location and weld toe were known, a scaling factor was determined for each boundary condition case analyzed. This scaling factor allowed the extrapolation of the stresses from the gage location to

the weld toe. Figure 4.1 below shows the location of the superimposed foil gage on the bottom connection model.

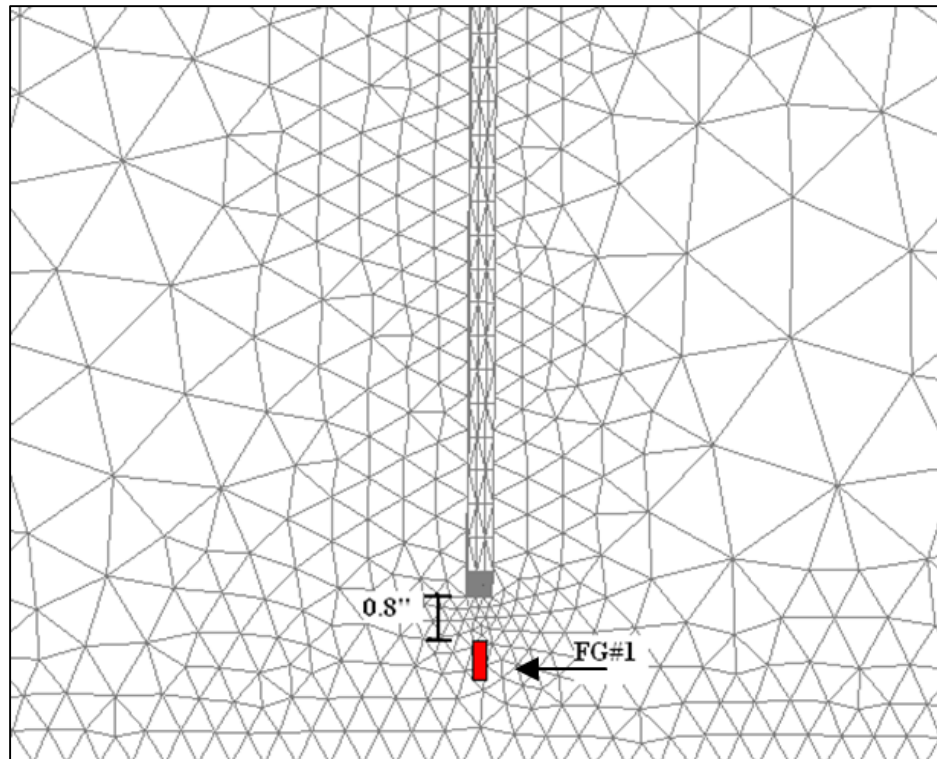


**Figure 4.1** Foil gage #1 field location superimposed on bottom web gap finite element model.

The finite element analysis results show that a very high stress gradient exists in the web gap region. However, the foil gage installed in the web gap region only provides a single strain output obtained by integrating strains over its entire length. In order to obtain a single strain value corresponding to the foil gage, the output at three nodal points along the superimposed length of the foil gage were recorded and averaged. The three nodal locations used corresponded to the top, middle

and bottom of the superimposed foil gage. The stress values obtained from these nodal locations are presented in Table 4.1 below.

**Table 4.1 Nodal stress ( $\sigma_y$ ) values obtained along superimposed foil gage length.**

Point along gage	Stress ( $\sigma_y$ )		
	All Fixed	Bottom & Sides Fixed	Bottom fixed
<b>Top</b>	2.98	3.52	3.98
<b>Mid</b>	2.34	3.11	0.789
<b>Bottom</b>	1.87	-0.275	-0.869
<b>Average</b>	2.40	2.12	1.30

Similarly to the boundary condition study carried out in Chapter 2 (see Table 2.2), scaling factors were determined for three sets of boundary conditions. The output of interest was the vertical or Y-component of the maximum principal stress. Table 4.2 on the next page, summarizes the  $\sigma_y$  stress output at the superimposed foil gage location and corresponding weld toe maximum stress.

**Table 4.2 Stress ( $\sigma_y$ ) at superimposed foil gage location and corresponding weld toe maximum stress ( $\sigma_y$ ) for varying boundary conditions.**

	<b>All fixed</b>	<b>Bottom &amp; Sides Fixed</b>	<b>Bottom Fixed</b>
<b>Superimposed FG#1 Location (ksi)</b>	2.40	2.12	1.77
<b><math>\sigma_y</math> at weld toe (ksi)</b>	25.11	28.57	32.45
<b>Scaling Factor</b>	10.46	13.48	18.33

The scaling factors shown in Table 4.2 were used in conjunction with Miner’s Rule and the Rainflow histogram results of the in-service monitoring (Table 3.3) to determine an effective stress at the weld toe of the bottom connection plate.

#### **4.3 Effective Stress ( $S_r$ )**

Given a variable amplitude loading in histogram form, Miner’s rule is used to calculate an “effective” stress. This is done by multiplying the cubed mid-width value of the interval (i) times the fraction of stress ranges in interval (i). This quantity is summed for all intervals and raised to the one-third power. The result is a single value representing an effective stress range for the given histogram.

$$S_r = \left( \sum_{i=1}^k f_i S_i^3 \right)^{\frac{1}{3}} \quad \text{Equation 4.2}$$

Since vehicles weighing less than 20 kips have a very low probability of causing fatigue damage (Alampalli, 2006), it becomes necessary to establish a minimum amplitude threshold when calculating the effective stress. The desired

outcome is to eliminate those cycles that are not causing any fatigue damage to the structure. Several different minimum stress cutoff values have been proposed to calculate an effective stress. Alampalli (Alampalli, 2006) suggest performing a controlled load test with a vehicle of known weight and scaling the recorded values to the equivalent of those caused by a 20 kip truck. Unfortunately, a controlled load test was not performed at the Newport Viaduct and the response caused by a known truck load is unavailable. Alternatively, Connor & Fisher (Connor & Fisher, 2006) and Zhou (Zhou, 2006) proposed using cutoff values of 0.25CAFT and 0.50CAFT respectively. Given a constant amplitude fatigue threshold of 10.0ksi for a Category C detail, these proposed cutoff points would be 2.5ksi and 5.0ksi.

Difficulties arise when attempting to use a single factor of the CAFT as the cutoff value to calculate the effective stress. Given the different scaling factors that arise from the various boundary conditions analyzed, it is unclear which single value of stress at the weld toe is the most accurate. In other words, the choice of boundary conditions significantly affects the magnitude of the stress at the weld toe thus making it impossible to use a single CAFT factor as the cutoff point. For this reason, it became necessary to calculate the effective stress for all boundary condition cases and their corresponding scaling factors. Instead of using a single factor of the CAFT as the effective stress cutoff value, the mid-width value of bins 2-7 of the Rainflow histogram (Table 3.3) was used. Table 4.3 on the next page summarizes the effective stress calculation results.

**Table 4.3 Effective Stress calculation results.**

Bin	Mε	Cut-off mid- bin stress $\sigma_{MB}$ (ksi)	Total # of Cycles	Cut-off stress at weld toe (ksi)			Effective Stress at weld toe (ksi)			
				All fixed (10.46* $\sigma_{MB}$ )	Bottom & Sides Fixed (13.48* $\sigma_{MB}$ )	Bottom Fixed (18.33* $\sigma_{MB}$ )	All fixed	Bottom & Sides Fixed	Bottom Fixed	Average
2	5-10	0.22	1,546,673	2.28	2.93	3.99	3.54	4.56	6.21	4.77
3	10-15	0.36	304,556	3.79	4.88	6.64	5.62	7.24	9.85	7.57
4	15-20	0.51	102,143	5.31	6.84	9.30	7.50	9.66	13.14	10.10
5	20-25	0.65	42,758	6.83	8.79	11.96	9.28	11.95	16.30	12.51
6	25-30	0.80	20,309	8.34	10.74	14.62	11.00	14.17	19.28	14.82
7	30-35	0.94	10,608	9.86	12.70	17.28	12.65	16.28	22.16	17.03

Given the large variability in the calculated effective stresses at the weld toe, mean fatigue life was calculated for each effective stress corresponding to the various boundary conditions.

#### **4.4 Lifetime Average Daily Truck Traffic (LADTT)**

Lifetime average daily truck traffic (LADTT) is a measure used in Equation 4.1 to quantify the number of cycles believed to cause fatigue damage. In order to calculate LADTT, yearly average daily truck traffic (ADTT) counts are averaged for the number of years the structure has been in service. Yearly ADTT counts dating to 1978 can be obtained by using present ADTT and an assumed growth rate. Previous fatigue life analysis done by Kucz (Kucz, 2009), used ADTT estimates provided by DelDOT with a 4% yearly exponential growth rate to calculate LADTT. In an attempt to be consistent, the same growth rate numbers are assumed for the present fatigue life analysis. Background information on LADTT estimates can be found in (Kucz, 2009).

Instead of using a present day ADTT estimate provided by DelDOT as the starting value, the current analysis used the number of cycles obtained from the Rainflow histogram in-service monitoring results. These numbers are believed to be a better representation of the number of load cycles experienced by the web gap detail as opposed to the bridge structure as a whole. The number of cycles for bins 2-7 (Table 4.3) was divided by 23, the length in days of the in-service monitoring period, to obtain an average daily “truck” traffic count. This present day ADTT was used to calculate LADTT assuming a 4% exponential growth rate. Table 4.4 on the next page shows the results of the LADTT calculations.

**Table 4.4 LADTT estimates with 4% exponential growth rate.**

Year	Average Daily Truck Traffic (ADTT)					
	Bin 2	Bin 3	Bin 4	Bin 5	Bin 6	Bin 7
2011	67,247	13,242	4,441	1,859	883	461
2010	64,661	12,733	4,270	1,788	849	443
2009	62,174	12,243	4,106	1,719	816	426
2008	59,782	11,772	3,948	1,653	785	410
2007	57,483	11,319	3,796	1,589	755	394
2006	55,272	10,884	3,650	1,528	726	379
2005	53,146	10,465	3,510	1,469	698	364
2004	51,102	10,063	3,375	1,413	671	350
2003	49,137	9,676	3,245	1,358	645	337
2002	47,247	9,304	3,120	1,306	620	324
2001	45,430	8,946	3,000	1,256	597	311
2000	43,682	8,602	2,885	1,208	574	299
1999	42,002	8,271	2,774	1,161	552	288
1998	40,387	7,953	2,667	1,116	530	277
1997	38,833	7,647	2,565	1,074	510	266
1996	37,340	7,353	2,466	1,032	490	256
1995	35,904	7,070	2,371	993	471	246
1994	34,523	6,798	2,280	954	453	237
1993	33,195	6,537	2,192	918	436	228
1992	31,918	6,285	2,108	882	419	219
1991	30,691	6,043	2,027	848	403	210
1990	29,510	5,811	1,949	816	387	202
1989	28,375	5,588	1,874	784	373	195
1988	27,284	5,373	1,802	754	358	187
1987	26,234	5,166	1,733	725	344	180
1986	25,225	4,967	1,666	697	331	173
1985	24,255	4,776	1,602	671	318	166
1984	23,322	4,593	1,540	645	306	160
1983	22,425	4,416	1,481	620	294	154
1982	21,563	4,246	1,424	596	283	148
1981	20,734	4,083	1,369	573	272	142
1980	19,936	3,926	1,317	551	262	137
1979	19,169	3,775	1,266	530	252	131
<b>LADTT</b>	38,460	7,573	2,540	1,063	505	264

The LADTT estimates shown in Table 4.3 vary greatly. The values range from an LADTT=30,887 for Bin 2 to an LADTT=119 for Bin 7. These extreme values are not realistic representations of the actual LADTT of the structure, but are presented herein nonetheless for completeness. In contrast to Table 4.3, southbound ADTT in 2007 was reported as 3,124 vehicles at the Newport Viaduct (Kucz, 2009). Using this number as a benchmark, it becomes apparent that the cycle counts of Bins 3 & 4 are in the same order of magnitude. While mean fatigue life calculations will be carried out for Bins 2-7, the results obtained from Bins 3 & 4 are expected to be the most realistic given the ADTT of the Newport Viaduct.

#### **4.5 Mean Fatigue Life Estimates**

Provisions in AASHTO's Fatigue Evaluation for Existing Steel Bridges (FEESB) (AASHTO, 1990) were used to determine the mean fatigue life of the connection plates at Type E diaphragms. While Equation 4.1 is primarily used to estimate the mean remaining fatigue of a detail, it can also be used to provide insight as to when fatigue crack formation began. To accomplish this, the "*a*" term in Equation 4.1 is taken as  $a=0$ . The result obtained is the number of years of service life of the structure until the first fatigue cracks formed.

The procedure outlined in AASHTO (1990) assumes trucks travel on the right lane of the structure. However, ADTT estimates account for traffic on all lanes of the bridge. Since an accurate measure of the distribution of trucks in the travel lanes is lacking, AASHTO proposes applying a lane reduction factor to the LADTT value used in Equation 4.1. The various possible values for this lane reduction factor are listed in Table 4.5 on the next page.

**Table 4.5** ADTT lane reduction factor from FEESB (AASHTO, 1990)

<b>Number of lanes</b>	<b>2-way traffic</b>	<b>1-way traffic</b>
1	n/a	1
2	0.6	0.85
3	0.5	0.8
4	0.45	0.8
5	0.45	0.8
6 or more	0.4	0.8

The southbound direction of the Newport Viaduct where the monitoring system was installed consisted of two lanes with 1-way traffic. Per Table 4.4, the lane reduction factor used in the fatigue life calculations was 0.85. The final input values used in Equation 4.1 are presented below. The values for effective stress range ( $S_r$ ) and LADTT ( $T_a$ ) were taken from Tables 4.3 and 4.4 respectively.

$$Y_f = \frac{(f = 2.0)(K = 12 \times 10^6)}{(0.85)(T_a)(C = 1)((R_s = 1)(S_r)^3) - (a = 0)}$$

Fatigue life calculations for all three boundary condition cases are presented on Table 4.6 on the next page.

**Table 4.6 Fatigue life calculations**

Bin	Total # of Cycles	ADTT	LADTT	Weld toe Effective Stress (ksi)			Mean Fatigue Life (years)			
				All fixed	Bottom & Sides fixed	Bottom fixed	All fixed	Bottom & Sides fixed	Bottom fixed	Average
2	1,546,673	67,247	38,460	3.54	4.56	6.21	16.5	7.7	3.1	9.1
3	304,556	13,242	7,573	5.62	7.24	9.85	21.0	9.8	3.9	11.6
4	102,143	4,441	2,540	7.5	9.66	13.14	26.3	12.3	4.9	14.5
5	42,758	1,859	1,063	9.28	11.95	16.3	33.2	15.6	6.1	18.3
6	20,309	883	505	11	14.17	19.28	42.0	19.7	7.8	23.2
7	10,608	461	264	12.65	16.28	22.16	52.8	24.8	9.8	29.1

As seen in Table 4.6, the mean fatigue life of the bottom web gap detail varies greatly depending on the effective stress cutoff value chosen and the boundary conditions applied. Mean fatigue life estimates range from a low of 3.1 years for Bin 2, bottom edge fixed to a high of 52.8 years for Bin 7, all edges fixed. Despite this seemingly large variation in the results, meaningful mean fatigue life estimates of the desired detail can still be obtained.

The seemingly large range of fatigue life results presented in Table 4.6 can be significantly narrowed down. Given the 2007 southbound ADTT of 3,124 vehicles, several of the results presented in Table 4.6 can be disregarded based on their ADTT estimates. The mean fatigue life results for Bin 2-3 and Bins 6-7 can be discounted given that their ADTT estimates are not in the same order of magnitude as the value provided by DeIDOT. Disregarding the results of these bins greatly reduces the range of mean fatigue life estimates for the bottom connection detail from a low of 4.9 years to a high of 33.2 years.

The results of Table 4.6 indicate that the choice of boundary conditions greatly influences the calculated mean fatigue life of the detail. This situation arises due to the presence of cubed effective stress term in Equation 4.1. Even seemingly small variations in the calculated effective stress value used lead to large differences in the mean fatigue life results. Precisely establishing which set of boundary conditions most closely resemble the field conditions around the boundaries of the finite element model is notably difficult and not the focus of this project. Moreover, this challenge is exacerbated by the fact that the actual field conditions are likely to be a combination of the various boundary condition cases analyzed herein. For this reason, no attempt was made to establish the “correct” set of boundary conditions. Instead, the mean

fatigue life results of all the boundary condition cases covering the spectrum of fixity were averaged and their results were tabulated on the rightmost column of Table 4.6.

After examining the averaged fatigue life results in Table 4.6, it becomes apparent that the values obtained from the bottom edge fixed boundary condition case are unrealistically low. The mean fatigue life estimate obtained from the bottom edge fixed boundary condition ranges from 3.1 years to 9.8 years for Bins 2-7. These results imply the first cracks would have formed in the 1980s. Had the fatigue cracks formed in the 1980s, the in-depth inspection in 2006 would have discovered extensive corrosion at the cracked locations and this was not the case. In other words, fixing the bottom edge of the model and allowing all other edges to rotate/displace freely does not approximate the field conditions and leads to fatigue life estimates that are too low. For this reason, the mean fatigue life results obtained from the bottom edge fixed boundary condition will be not be considered.

After discarding the fatigue life estimates from the bottom edge boundary condition case and averaging the results of the other two boundary condition sets for Bins 4-5 the result is a relatively narrow range of fatigue life estimates. The final fatigue life estimates are presented on Table 4.7 on the next page. The average of the results in Bin 4 provides a low fatigue life estimate of 19.3 years while the average of the results in Bin 5 provides a high fatigue life estimate of 24.4 years. Considering that the DeIDOT ADTT estimate for 2007 falls in between the cycle counts of Bins 4 & 5, it follows that the fatigue life estimate should also fall in between the values from these two bins. Accordingly, calculating the average of all the fatigue life estimates in Table 4.7 leads to a mean fatigue life of 22 years for the bottom web gap detail.

The mean fatigue life estimated from the cycle counts and effective stresses of Bins 4 & 5 is 22 years. In the context that fatigue cracks were discovered at the Newport Viaduct during an inspection in 2006, this value of fatigue life estimate is not unreasonable. This result suggests that fatigue cracks started to form at the bottom connection detail around the year 2000. This result is based on the mean fatigue life estimate. It is expected that some percentage of the cracks formed before the year 2000, and some percentage of the cracks probably formed after the year 2000. Furthermore, the lack of extensive corrosion at cracked web gap details suggest that these areas have not been exposed to the elements for extended periods of time. For these reasons, the mean fatigue life estimate of 22 years for the bottom web gap detail seems fitting. Table 4.7 below shows the final fatigue life estimates used.

**Table 4.7 Fatigue life estimates**

Bin	Total # of Cycles	ADTT	LADTT	Weld toe Effective Stress (ksi)		Mean Fatigue Life (years)		
				All fixed	Bottom & Sides fixed	All fixed	Bottom & Sides fixed	Average
4	102,143	4,441	2,540	7.5	9.66	26.3	12.3	19.3
5	42,758	1,859	1,063	9.28	11.95	33.2	15.6	24.4

Instead of attempting to narrowly determine the exact date of crack formation, this study focuses on the broader implications. It has previously been established that the bottom connection web gap experiences larger stresses. Its estimated mean fatigue life is approximately 22 years, which suggests fatigue cracks

started to form around the year 2000. While not all bottom web gap details have shown the presence of fatigue cracks, the results of this study suggest that crack formation in the remaining uncracked details is imminent.

## Chapter 5

### CONCLUSIONS AND RECOMMENDATIONS

#### 5.1 Summary and Conclusions

DelDOT bridge 1-501, also known as the Newport Viaduct is a twin span trapezoidal box girder bridge with an approximate length of 1,984 feet located in Newport, DE. A 2006 in depth inspection of the inside of the box girders revealed the presence of 665 fatigue cracks near the internal Type E diaphragms. The cracks were located in an unstiffened 2.5 inch area between the termination of the diaphragm connection plate and top and bottom flanges of the box girder known as the web gap region. This particular web gap detail is a widely documented fatigue prone detail. Due to the lack of positive attachment between the diaphragm connection plate and the flanges of the girder, this web gap detail is subject to out of plane deformations which lead to the formation of distortion induced fatigue cracks. The driving force behind the formation of the cracks is the out of plane distortion in the web gap region, while longitudinal bending of the girders is believed to have a negligible effect.

A joint venture research project was established between DelDOT, AECOM and the University of Delaware to further study the fatigue cracks at the Newport Viaduct. Two previous graduate students authored Masters Theses focusing on the Newport Viaduct. Work done by Kucz (Kucz, 2009) and Quiqley (Quiqley, 2009) consisted of creating global finite element models of portions of the bridge to provide fatigue life estimates and validate the effectiveness of various retrofit options respectively. The finite element models used in these projects were calibrated through

a field test. Results from these projects estimated the fatigue life of the structure between 27-32 years and recommended the positive attachment of the connection plate to the flanges as the best retrofit option.

In continuation of previous work done, it was desired to record the response of the Newport Viaduct caused by everyday traffic loads and use these values to carry out a fatigue analysis. Strain data obtained from this monitoring period was used to estimate the average daily truck traffic (ADTT) and the effective stress at the weld toe of the connection plate. These values were used in conjunction with AASHTO's Fatigue Evaluation of Existing Steel Bridges (AASHTO, 1990) to obtain estimates of the mean fatigue life of the web gap details.

In order to understand the stress distribution in the web gap details, localized finite element models of the web gap regions were created. Differences in the geometry of the top and bottom connection details suggested that a single finite element model would be unable to accurately model both regions. For this reason, two distinct localized finite element models were created. Instead of establishing a single set of boundary conditions, the models were analyzed for three distinct sets. Three boundary conditions ranging from all edges fixed to only the top/bottom edge fixed were analyzed for each model. Analysis results showed a very high maximum principal stress gradient in the web gap region as expected. Moreover, the results showed that the bottom web gap detail experienced higher stresses than the top web gap detail for a given loading.

The bolt holes configuration in the top and bottom connection is believed to have an impact on the resultant stresses at the weld toe. The centroid of the bolt holes in the bottom connection coincides with the line of action of the cross frame

angle resulting in a strictly shear loading of the bolts. On the other hand, the centroid of the top connection bolt holes does not coincide with the line of action of the cross frames. This situation is believed to cause bending in addition to the shear at the connection. Thus, the applied loads in the top connection are likely resisted not only the shear capacity of the bolts, but also by an internal couple created by the geometric configuration of the bolt holes. The overall result is that less load is likely transferred to the top connection plate, possibly resulting in smaller out of plane deformations. In addition, the proximity of the composite deck to the top web gap region together with the presence of the transverse L7x4x $\frac{3}{8}$  angle is believed to provide additional rigidity to this region. A top web gap with greater stiffness than the bottom web gap is expected to undergo smaller out of plane deformations resulting in smaller stresses at the weld toe and possibly have a larger fatigue life. As such, this study focused on determining the fatigue life of the bottom web gap as it is expected that this detail will control the fatigue life of the overall structure.

In-service monitoring of the Newport Viaduct was carried for 23 days between November 17, 2010 and December 10, 2010. The monitoring system was installed near the second Type E diaphragm of the exterior box girder of span 10 southbound. The monitoring system consisted of two resistive foil type strain gages installed directly in the web gap region and six BDI strain transducers installed at locations. Power was supplied to the system by two 12V batteries and measurements were recorded and processed using a Campbell Scientific CR5000 datalogger. The data recorded during this period included minute-interval maximum/minimum values and Rainflow histograms for each gage. These values were used to determine the response of the structure to traffic loads and to count the number of load cycles

experienced. In addition, on the morning of December 14<sup>th</sup>, data was recorded at 100Hz for a period of approximately three hours. This data was used to generate snapshots of the overall response of the bridge centered around load peaks. These snapshots provided insight into the instantaneous structural response of the Newport Viaduct to significant loads.

Post completion of the in-service monitoring, it became necessary to determine the stresses at the weld toe of the bottom web gap region. The localized finite element models were used to establish scaling factors between the foil gage location in the web gap region and the corresponding maximum stress at the weld toe. Different scaling factors were obtained for each of the boundary condition sets analyzed. These various scaling factors resulted in a large range of estimates for stress magnitude at the weld toe as a function of the boundary condition applied. Given this large variation, Miner's rule and the Rainflow histogram cycle count results were applied to each boundary condition case to determine an effective stress at the weld toe.

The cycle counts obtained from the Rainflow histogram were used as a proxy measure for average daily truck traffic (ADTT) counts. The cycle count values obtained during the monitoring period were divided by 23 days to obtain a corresponding ADTT value. Instead of trying to establish a single correct ADTT from the Rainflow histogram results, the cycle counts of Bins 2-7 were used. This resulted in six present day ADTT estimates. A 4% yearly exponential growth was assumed to be consistent with previous work done by Kucz (Kucz, 2009). Using this growth estimate, ADTT counts were calculated for every year since the opening of the Newport Viaduct in 1978. These yearly ADTT values were averaged to obtain a

Lifetime Average Daily Truck Traffic (LADTT) value for the service life of the structure. Since this procedure was carried out for six ADTT estimates from Bins 2-7, the result was six LADTT values which were later used in the fatigue life calculation.

The mean fatigue life of the bottom connection detail was calculated following the method outlined in FEESB (AASHTO, 1990). Fatigue life estimates were calculated for the numerous effective stress values obtained from the application of different boundary conditions and for the cycle counts of Bins 2-7. This resulted in a very large range of predictions for mean fatigue life. Using the ADTT traffic count provided by DeIDOT for 2007, many of the fatigue life results were disregarded based on their ADTT estimates. Following this approach, the fatigue life estimates obtained from the cycle counts of Bin 2-3 and Bins 6-7 were discarded. Moreover, the fatigue life estimates obtained from the bottom edge fixed boundary condition were also discarded given that they were unrealistically low.

The mean fatigue life results for Bin 4 & 5 ranged from a low of 12.3 years to a high of 33.2 years based on the boundary condition set applied. Given that the actual fixity field condition around the edge of the localized models is likely a combination of the boundary conditions analyzed herein, the average of the fatigue life results was calculated. The result is that the mean fatigue life of the bottom web gap is predicted to be 22.0 years. Since the Newport Viaduct has been in service since 1978, the results of this analysis predict the first formation fatigue cracks in the year 2000. Given that fatigue cracks were detected during an inspection in 2006, this fatigue life estimate is not unreasonable.

Building upon previous research done on the Newport Viaduct, this project has produced significant new contributions. The creation of localized finite

element models led to the breakthrough that the bottom and top connection details did not exhibit the same structural response. Specifically, the bottom connection detail experienced a higher stress in the web gap region than the top connection detail for the same loading. This higher state of stress at the bottom web gap would result in a lower fatigue life. This finding is consistent with the observation that 75% of the cracks identified in the 2006 bridge inspection report were located in the bottom web gap region. In addition, the in-service monitoring of the Newport Viaduct for 23 days provided very useful data. Instead of relying on an ADTT estimate, the actual number of load cycles in the web gap region was recorded using the Rainflow algorithm. This cycle count was used to calculate an effective stress and mean fatigue life at the bottom web gap. Improving upon previous work done, the mean fatigue life results presented herein are believed to be more accurate given that they were calculated using field data measured during the in-service monitoring period.

## **5.2 Recommendations**

The fatigue life results suggest that the formation of the first fatigue cracks at the bottom web gap detail occurred around the year 2000; some may have formed before that time and others formed after that averaged estimated time. Moreover, it implies that current uncracked bottom web gap details are likely to crack in the nearby future. As such, a timely retrofitting strategy of both web gap details is necessary to arrest the fatigue cracking and prevent further structural damage. Given the findings of this study and the fact that 75% of the cracks in the 2006 inspection report occurred at the bottom web gap detail, retrofit priority should be given to the bottom web gap detail.

## REFERENCES

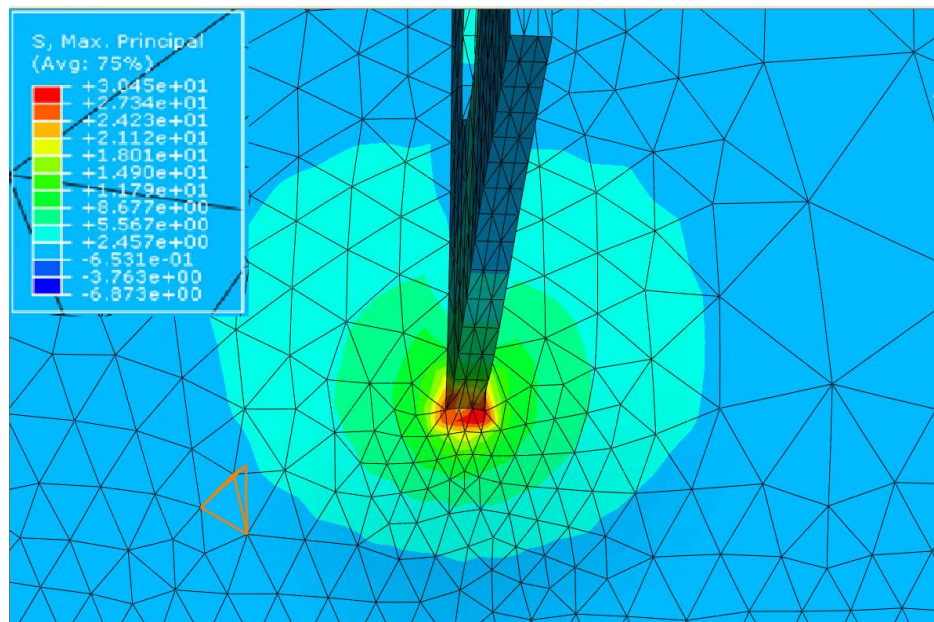
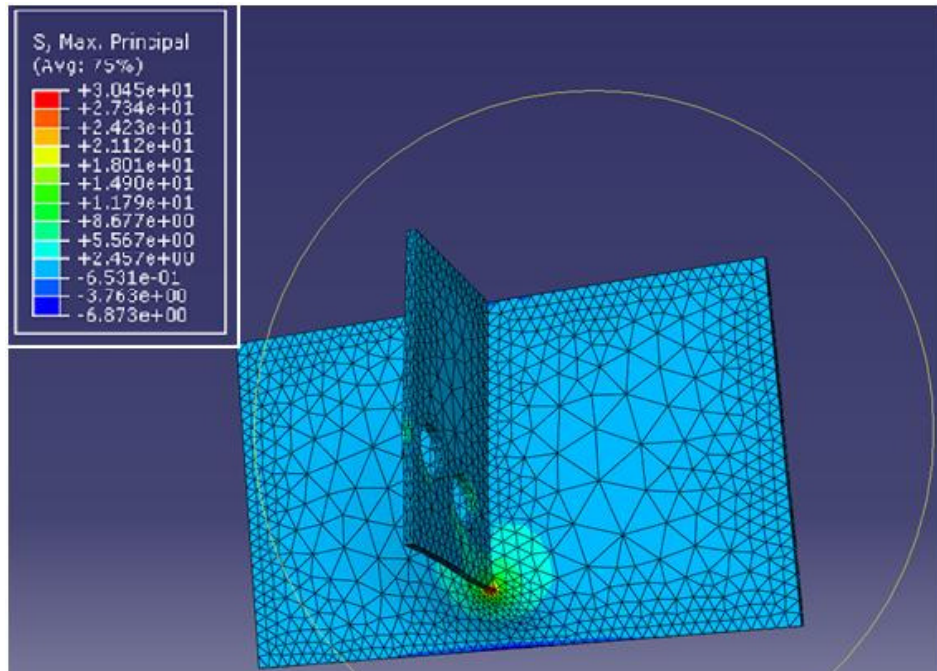
- AASHTO (1990). *Guide specifications for fatigue evaluation of existing steel bridges*, American Association of State Highway and Transportation Officials, Washington, D.C.
- AASHTO (2010). *LRFD Bridge Design Specifications*, 5<sup>th</sup> Edition, American Association of State Highway and Transportation Officials, Washington, D.C.
- ABAQUS (2008). *ABAQUS/Standard Analysis User's Manual*. Version 6.7. Simulia, Inc.
- Alampalli, S. and Lund R. (2006). "Estimating Fatigue Life of Bridge Components Using Measured Strains." *Journal of Bridge Engineering*, 11(6), 725-736.
- ASTM Standard. (1997). "Standard Practices for Cycle Counting in Fatigue Analysis." E 1049-85 (Reapproved 2005). American Society for the Testing of Materials.
- Bridge Diagnostics (2006). "BDI Strain Transducer ST-350 specifications sheet". Bridge Diagnostics, Inc.
- Campbell Scientific (2006). "CR5000 Measurement and Control System Operator's Manual." Revision 11/06. Campbell Scientific, In.
- Campbell Scientific (2008). "RTDAQ version 1.0 specifications sheet." Campbell Scientific, Inc.
- Campbell Scientific (2009). "RavenXTV CDMA Sierra Wireless Cellular Modem User's Manual". Revision 3/09. Campbell Scientific, Inc.
- Campbell Scientific (2009). "Terminal Input Modules (TIMs) specification sheet." Campbell Scientific, Inc.
- Connor, R. J. and Fisher, J. W. (2006). "Identifying Effective and Ineffective Retrofits for Distortion Fatigue Cracking in Steel Bridges Using Field Instrumentation" *Journal of Bridge Engineering*, 11(6), 745-752.
- DMJM Harris, Inc. (2006). "SR-141 Newport Viaduct 2006 Initial Interior Box Inspection Report." Prepared for the Delaware Department of Transportation.
- Fisher, J. W. and Keating, P. B. (1989). "Distortion induced fatigue cracking of bridge details with web gaps." *Journal of Constructional Steel Research*, 12, 215-228.
- Fisher, J. W. (1984). *Fatigue and fracture in steel bridges: Case Studies*, John Wiley & Sons, New York.

- Jajich, D. and Schultz, A. E. (2003). "Measurement and Analysis of Distortion-Induced Fatigue in Multigirder Steel Bridges." *Journal of Bridge Engineering*, 8(2), 84-91.
- Kucz, D. (2009). "Analysis of Distortion Induced Fatigue Cracking in a Steel Trapezoidal Box Girder Bridge." University of Delaware.
- Kulak, G. and Wu, E. (1997). "Shear Lag in Bolted Angle Tension Members." *Journal of Structural Engineering*, 123(9), 1144-1152
- Micromeritics (2010). "General Purpose Sensor – Linear Pattern specification sheet." Vishay Precision Group, Inc.
- Quiqley, J. (2009). "Analysis of Distortion-Induced Fatigue Cracking of a Trapezoidal Steel Box Girder Bridge Including Retrofit Investigation." University of Delaware.
- Roddis, W. M. K. and Zhao, Y. (2003). "Finite-Element Analysis of Steel Bridge Distortion-Induced Fatigue." *Journal of Bridge Engineering*, 8(5), 259-266.
- Vishay Micro-Measurements (2007). "*Strain Gage Thermal Output and Gage Factor Variation with Temperature.*" Tech Note TN-504-1. Vishay Precision Group, Inc.
- Zhou, E. (2006). "Assessment of Bridge Remaining Fatigue Life through Field Strain Measurement." *Journal of Bridge Engineering*, 11(6), 737-744.
- Zhu, H. T., Yam, M. C. H and Lam, A. C. C. (2009). "The shear lag effects on welded steel single angle tension members." *Journal of Constructional Steel Research*, (65), 1171-1186.

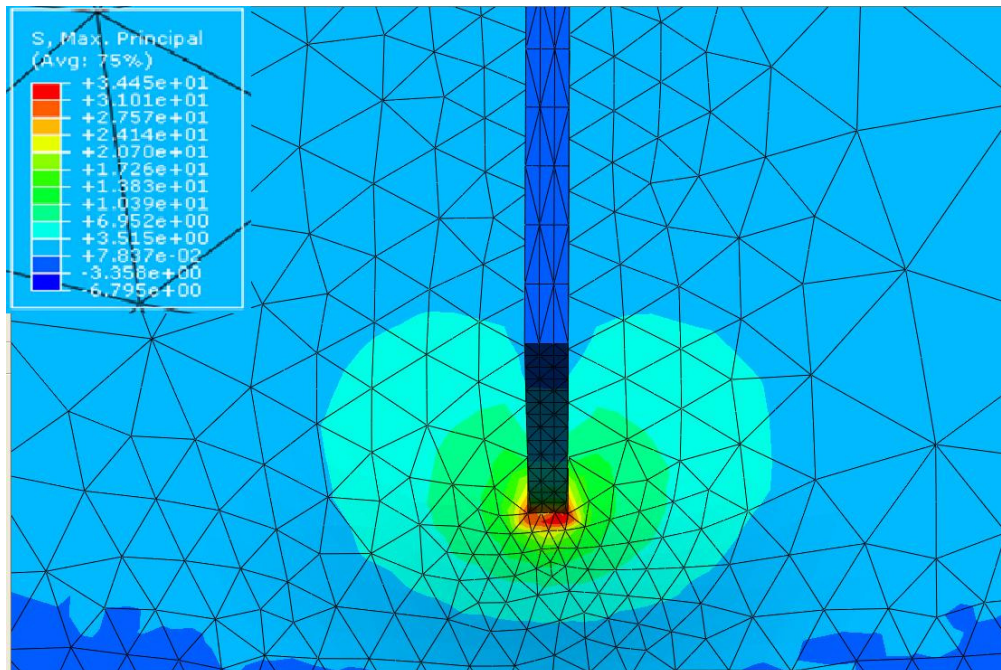
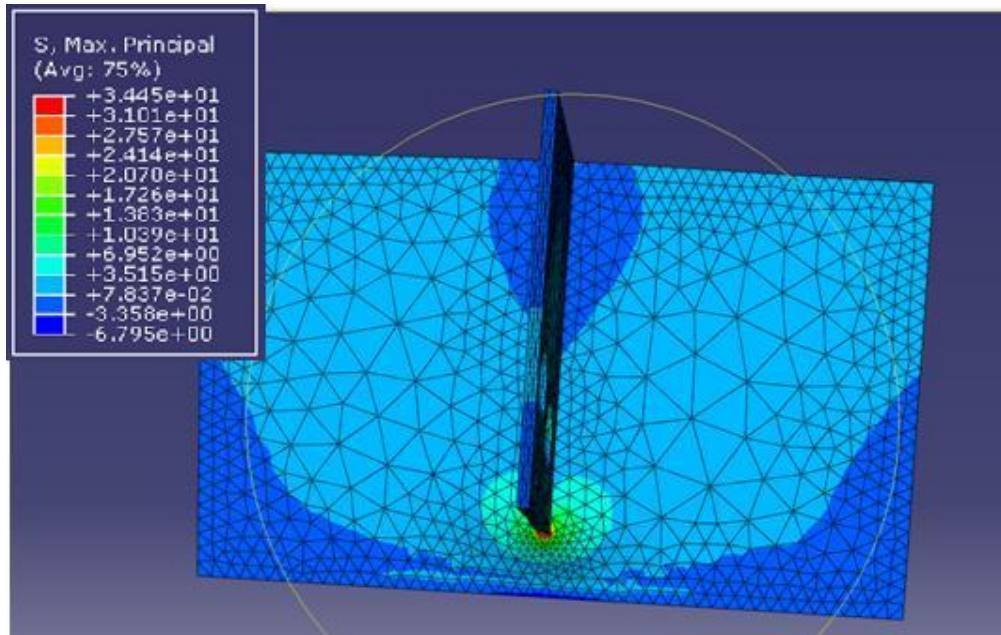
## **APPENDIX A. FINITE ELEMENT ANALYSIS OUTPUT**

The outputs of the various finite element analyses are presented herein. Given the large number of nodal values each model has, only graphical output results are presented.

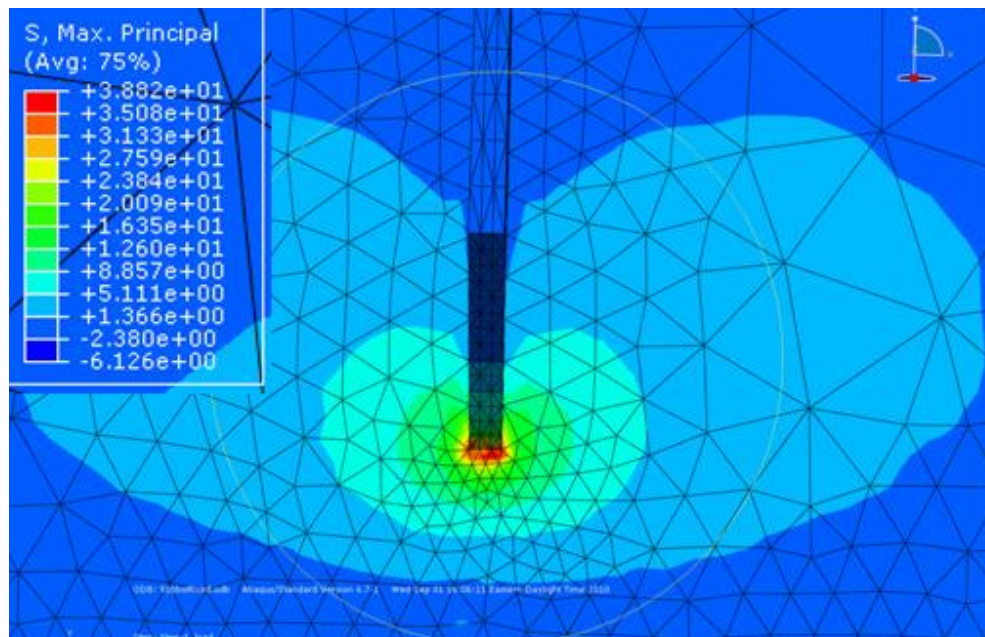
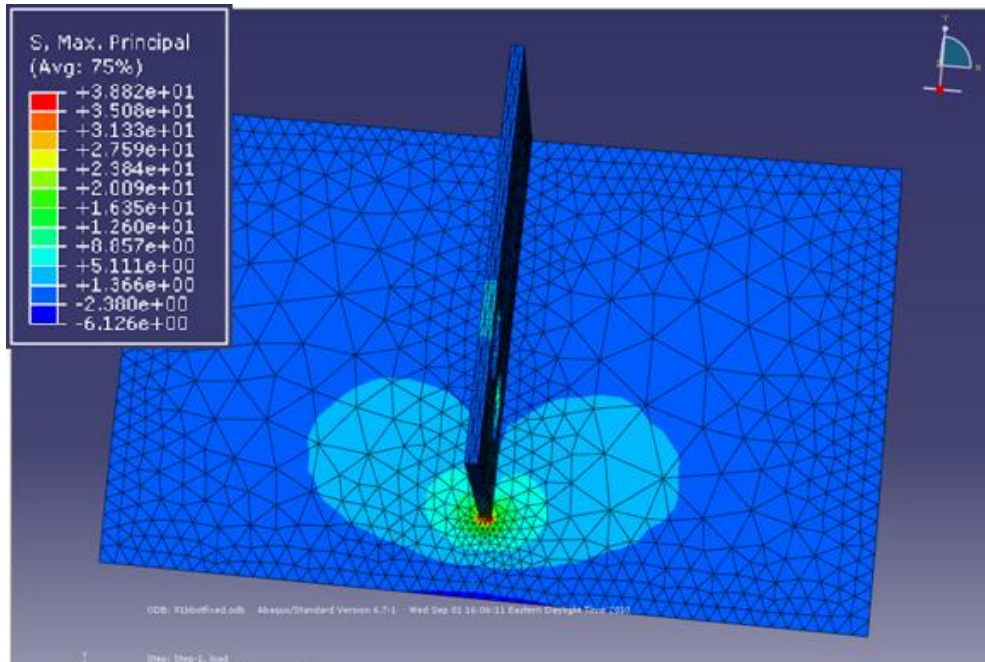
Bottom connection, all edges fixed.



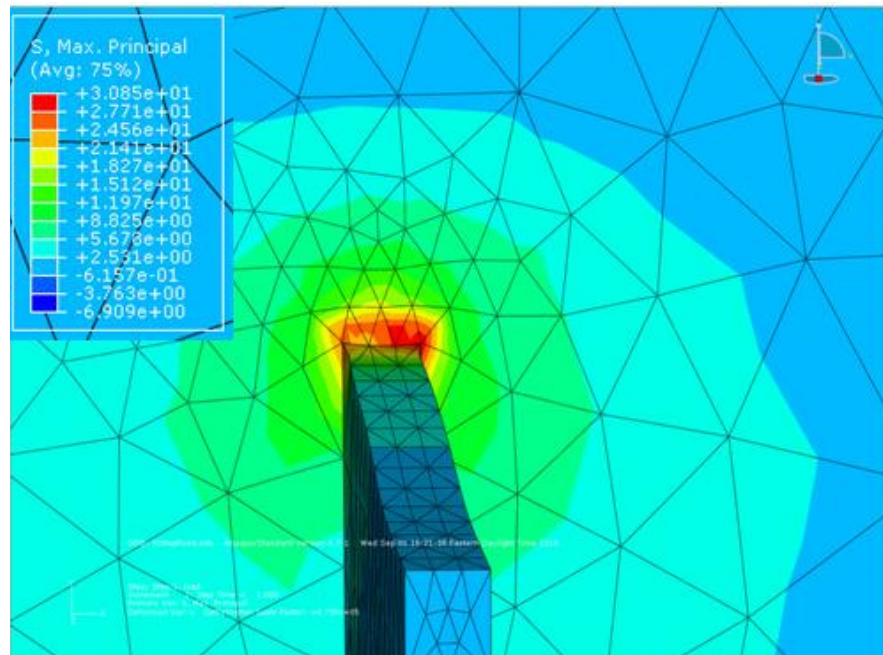
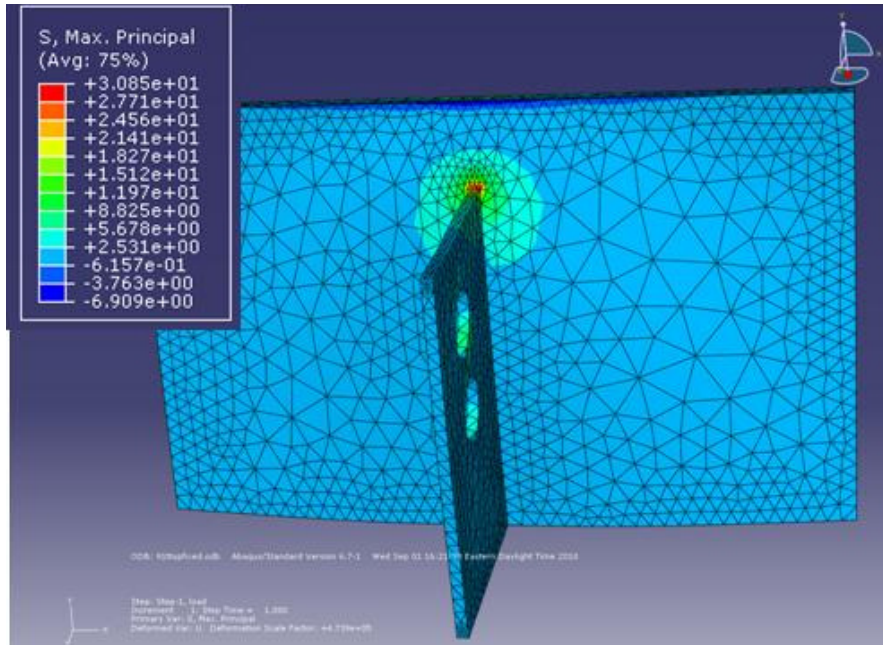
Bottom connection, sides and bottom fixed



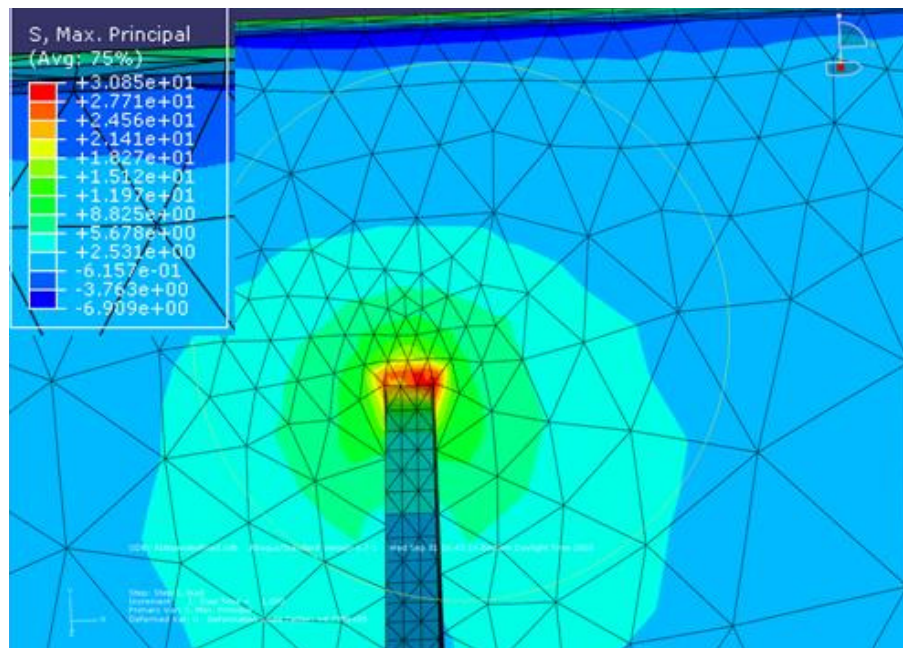
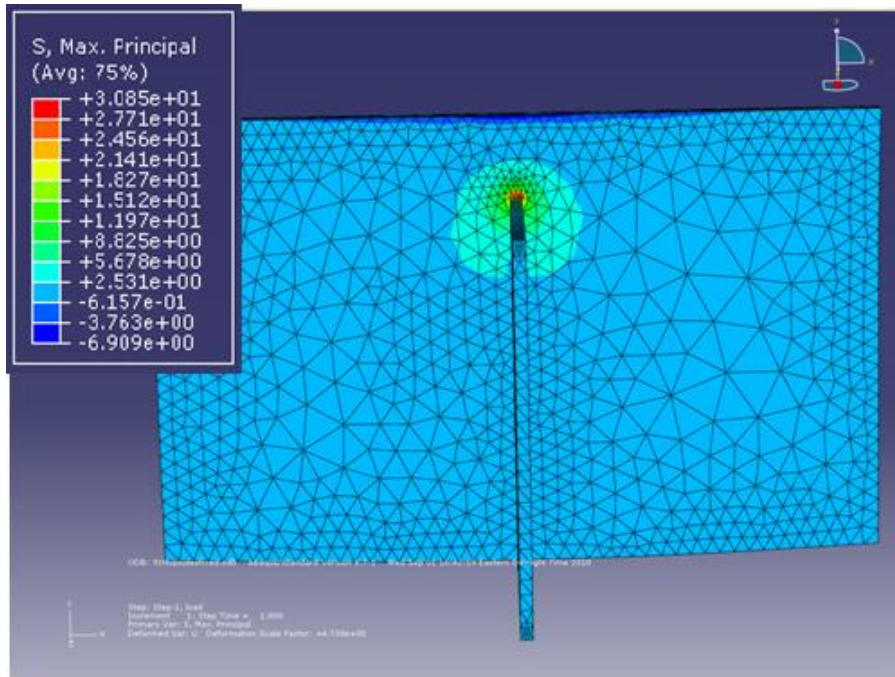
Bottom connection, bottom edge fixed



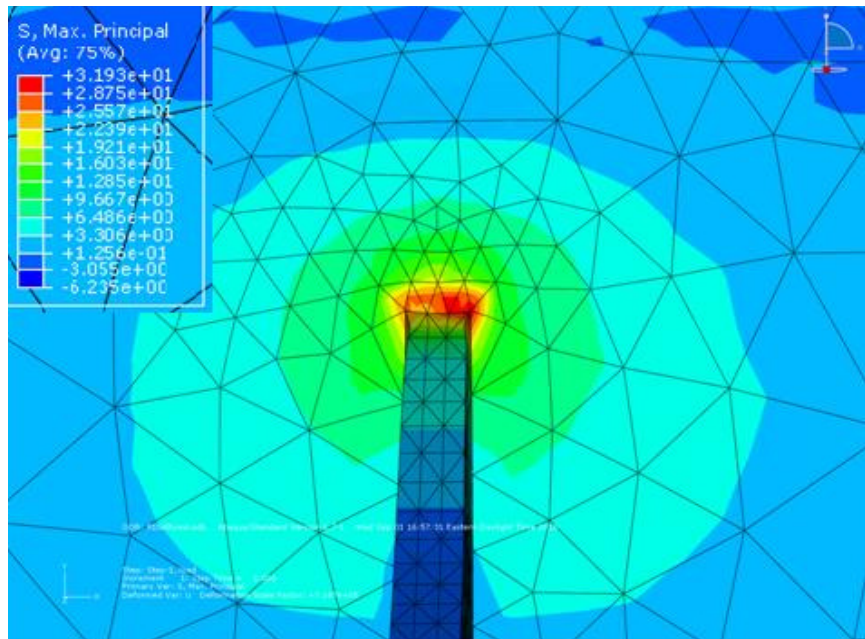
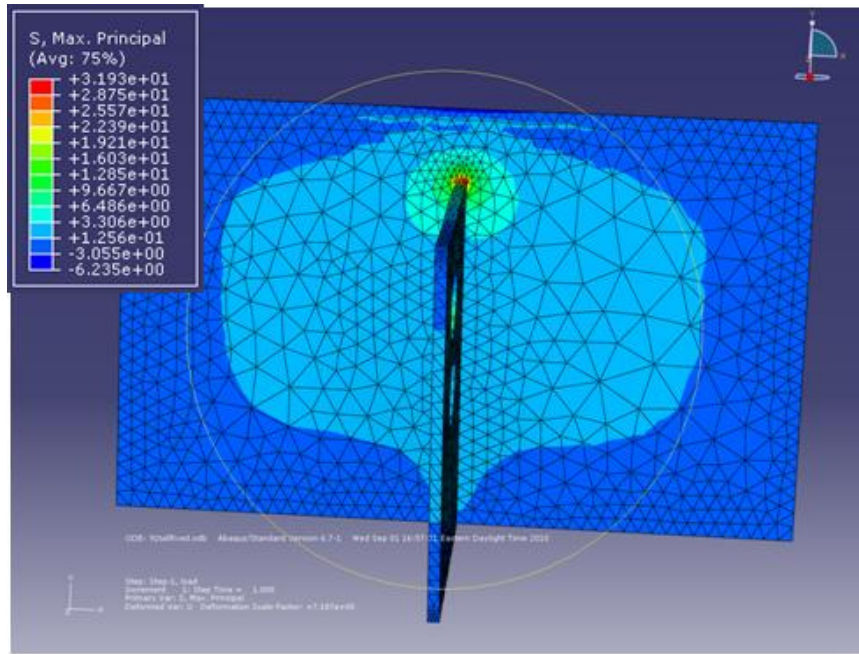
Top connection, top edge fixed



Top connection – Top and sides fixed



Top connection – All edges fixed



## **APPENDIX B. RTDAQ PROGRAMMING CODE**

The complete programming code used to control the CR5000 datalogger is presented herein. The code was generated using the Program Generator module within RTDAQ and edited in the CRBasic Editor module to include the instructions to selectively power the cellular modem. The wiring diagram for the strain gages is also included.

```

'          Program name: 8 GE_RAIN_RAWDATA.CR5
'          Written by: Jose
'          I.D. number: 1
'          Date written: 11-16-2010
'          Time written: 13:05:25
'          RT5GEN Version: 6.0.0066

```

```

' This program was generated using Campbell Scientific's RT5GEN
' Program Generator for the CR5000 Measurement & Control System.

```

```

'//////////////////////////////////// TIMING CONSTANTS //////////////////////////////////////

```

	Const PERIOD = 10	'Scan interval number
(mSecs)	Const P_UNITS = 1	'Scan interval units
number	Const INTERVAL1 = 60	'Table 1 interval
(Secs)	Const UNITS1 = 2	'Table 1 interval units
number	Const INTERVAL2 = 30	'Table 2 interval
(Mins)	Const UNITS2 = 3	'Table 2 interval units
number	Const INTERVAL3 = 10	'Table 3 interval
(Mins)	Const UNITS3 = 3	'Table 3 interval units
number	Const INTERVAL4 = 10	'Table 4 interval
(mSecs)	Const UNITS4 = 1	'Table 4 interval units

```

'//////////////////////////////////// BRIDGE CONSTANTS //////////////////////////////////////

```

```

' _____ Bridge Block 1
|
|_____
|
| Const BRNG1 = 4           'Block1 measurement
| range (mSecs)
| Const BREP1 = 2         'Block1 repetitions

```

	Const BEXCIT1 = 5000	'Block1 excitation
mVolts		
	Const BSETL1 = 200	'Block1 settling time
(usecs)		
	Const BINT1 = 100	'Block1 integration time
(usecs)		
	Const BGF1 = 2	'Block1 gauge factor
	Const BCODE1 = -1	'Block1 gauge code for
1/4 bridge strain		
	Const BMULT1 = 1	'Block1 default
multiplier		
	Const BOSET1 = 0	'Block1 default offset
	Public BBlk1(BREP1)	'Block1 dimensioned
source		
	Public BBlk1mV_V(BREP1)	
	Public GBBlk1Raw(BREP1)	
	Public GBBlk1(BREP1)	'Block1 dimensioned
gauge factor		
	Public BBlk1ZeroMv(BREP1)	'Block1 zero mV
variable		
	Public BCalMode1	
	Public BKnownVar1(BREP1)	
	Public BCalReps1	
	Units BBlk1ZeroMv = mVperV	'Block1 default
units (mVperV)		
	Units BBlk1 = uStrain	'Block1 default units
(uStrain)		
	' _____ Bridge Block 2	
	Const BRNG2 = 3	'Block2 measurement
range (mSecs)		
	Const BREP2 = 6	'Block2 repetitions
	Const BEXCIT2 = 5000	'Block2 excitation
mVolts		
	Const BSETL2 = 200	'Block2 settling time
(usecs)		
	Const BINT2 = 100	'Block2 integration time
(usecs)		
	Const BMULT2 = 1	'Block2 default
multiplier		
	Const BOSET2 = 0	'Block2 default offset
	Public BBlk2(BREP2)	'Block2 dimensioned
source		

```

        Dim MBBlk2(BREP2)                                'Block2 dimensioned
multiplier
        Dim OBBlk2(BREP2)                                'Block2 dimensioned
offset
        Public BBlk2ZeroMv(BREP2)                        'Block2 zero mV
variable
        Public BCalReps2
        Units BBlk2ZeroMv = mVperV                        'Block2 default
units (mVperV)
        Units BBlk2 = mVoltPVolt                          'Block2 default units
(mVoltPVolt)

```

\\\\\\\\\\\\\\\\\\\\ ALIASES & OTHER VARIABLES \\\\\\\\\\\\\\\\\

```

        Alias BBlk1(1) = Foil_gauge1                      'Assign alias name
"Foil_gauge1" to BBlk1(1)
        Alias BBlk1(2) = Foil_gauge2                      'Assign alias name
"Foil_gauge2" to BBlk1(2)
        Alias BBlk2(1) = BDI_303                          'Assign alias name
"BDI_303" to BBlk2(1)
        Alias BBlk2(2) = BDI_292                          'Assign alias name
"BDI_292" to BBlk2(2)
        Alias BBlk2(3) = BDI_2171                         'Assign alias name
"BDI_2171" to BBlk2(3)
        Alias BBlk2(4) = BDI_338                          'Assign alias name
"BDI_338" to BBlk2(4)
        Alias BBlk2(5) = BDI_356                          'Assign alias name
"BDI_356" to BBlk2(5)
        Alias BBlk2(6) = BDI_318                          'Assign alias name
"BDI_318" to BBlk2(6)

```

```

        Public Flag(8)                                     'General Purpose Flags
        Public ScanFlg1x(8) As Boolean
        Public FlagMode1
        Dim BattVolt                                       'Battery voltage
        Units BattVolt = Volts                             'Battery voltage units
        Dim I                                               'Declare I as a variable

```

\\\\\\\\\\\\\\\\\\\\ FIELD CALIBRATION GLOBAL VARIABLES \\\\\\\\\\\\\\\\\

```

        Public CalFileLoaded As Boolean
        Public CalStartIdx
        Const ZeroingCalib = 0
        Const CalStrainZero = 10
        Const Strain1_4Shunt = 13
        Public FieldCalAvgs

```

//////////////////////////////////// OUTPUT SECTION //////////////////////////////////////

```

'----- Table 1-----
DataTable(VALUES,True,-1)                                'Trigger, auto size
  DataInterval(0,INTERVAL1,UNITS1,100)                  '60 Sec
interval, 100 lapses, autosize
  CardOut(0,-1)                                          'PC card , size Auto
  '----- Bridge Blocks
-----
  Maximum(BREP1,BBlk1(),IEEE4,False,False)             '2
Reps,Source,Res,Enabled,Time of Max
  Minimum(BREP1,BBlk1(),IEEE4,False,False)             '2
Reps,Source,Res,Enabled,Time of Min
  Maximum(BREP2,BBlk2(),IEEE4,False,False)             '6
Reps,Source,Res,Enabled,Time of Max
  Minimum(BREP2,BBlk2(),IEEE4,False,False)             '6
Reps,Source,Res,Enabled,Time of Min
  EndTable                                              'End of table VALUES

'----- Table 2-----
DataTable(BAT,True,-1)                                  'Trigger, auto size
  DataInterval(0,INTERVAL2,UNITS2,100)                  '30 Min
interval, 100 lapses, autosize
  CardOut(0,-1)                                          'PC card , size Auto
  '----- Logger Power
-----
  Sample (1,BattVolt,FP2)                               '1 Reps,Source,Res
  EndTable                                              'End of table BAT

'----- Table 3-----
DataTable(RAINFLOW,True,-1)                            'Trigger, auto
size
  DataInterval(0,INTERVAL3,UNITS3,100)                  '10 Min
interval, 100 lapses, autosize
  CardOut(0,-1)                                          'PC card , size Auto
  '----- Bridge Blocks
-----
  RainFlow(BBlk1(1),IEEE4,False,1,38,20,400,10,110)
  RainFlow(BBlk1(2),IEEE4,False,1,38,20,400,10,110)
  RainFlow(BBlk2(1),IEEE4,False,1,38,20,400,10,110)
  RainFlow(BBlk2(2),IEEE4,False,1,38,20,400,10,110)
  RainFlow(BBlk2(3),IEEE4,False,1,38,20,400,10,110)

```



```

        MBBlk2(2) = -591.9                                'Exception multiplier for
BBlk2(2) alias "BDI_292"
        MBBlk2(3) = -541.5                                'Exception multiplier for
BBlk2(3) alias "BDI_2171"
        MBBlk2(4) = -646.9                                'Exception multiplier for
BBlk2(4) alias "BDI_338"
        MBBlk2(5) = -698.8                                'Exception multiplier for
BBlk2(5) alias "BDI_356"
        MBBlk2(6) = -602.8                                'Exception multiplier for
BBlk2(6) alias "BDI_318"
.....
    For I = 1 To 8
        ScanFlg1x(I) = True
    Next I

    For I = 1 To BREP1
        GBBlk1Raw(I) = GBBlk1(I)
    Next I
    BCalReps2 = BREP2

    CalFileLoaded = false
    CalFileLoaded = LoadFieldCal(1)
    FieldCalAvgs = 1
    CalStartIdx = 1

    Scan(PERIOD,P_UNITS,0,0)                                'Scan once every
10 mSecs, non-burst
    Battery(BattVolt)                                        'Battery voltage
measurement

    If Flag(1) Then
        If ScanFlg1x(1) Then
            CalStartIdx = 1
            BCalReps1 = BREP1
            BCalReps2 = BREP2
            FlagMode1 = 1
            ScanFlg1x(1) = False
        EndIf
        If (FlagMode1 <= 0) or (FlagMode1 = 6) Then Flag(1) = 0
    Else
        ScanFlg1x(1) = True
    EndIf

```

\_\_\_\_\_ Bridge Blocks

BrFull(BBlk1mV\_V(),BREP1,BRNG1,1,VX1,2,BEXCIT1,False,True,BSETL1,BINT1,1,BOSET1) 'Strain

StrainCalc(BBlk1(),BREP1,BBlk1mV\_V(),BBlk1ZeroMv(),BCODE1,GBBlk1(),0)  
'Strain calculation

BrFull(BBlk2(),BREP2,BRNG2,3,VX2,3,BEXCIT2,False,True,BSETL2,BINT2,MBBlk2(),OBBlk2())

FieldCalStrain(Strain1\_4Shunt,BBlk1(),1,GBBlk1(),0,BCalMode1,BKnownVar1(),CalStartIdx,FieldCalAvg,GBBlk1Raw(),0)

FieldCalStrain(CalStrainZero,BBlk1mV\_V(),BCalReps1,0,BBlk1ZeroMv(),FlagMode1,0,CalStartIdx,FieldCalAvg,0,BBlk1())

FieldCal(ZeroingCalib,BBlk2(),BCalReps2,0,OBBlk2(),FlagMode1,0,CalStartIdx,FieldCalAvg)

CallTable(CalHist)

\_\_\_\_\_ Output Table Control

CallTable VALUES

CallTable BAT

CallTable RAINFLOW

CallTable RAWVALUE

If IfTime(13,24,4) Then SW12(1) 'Turn the SW12  
switch on at a certain time

If IfTime(14,24,4) Then SW12(0) 'Turn the SW12  
switch off 2 hours after being turned on

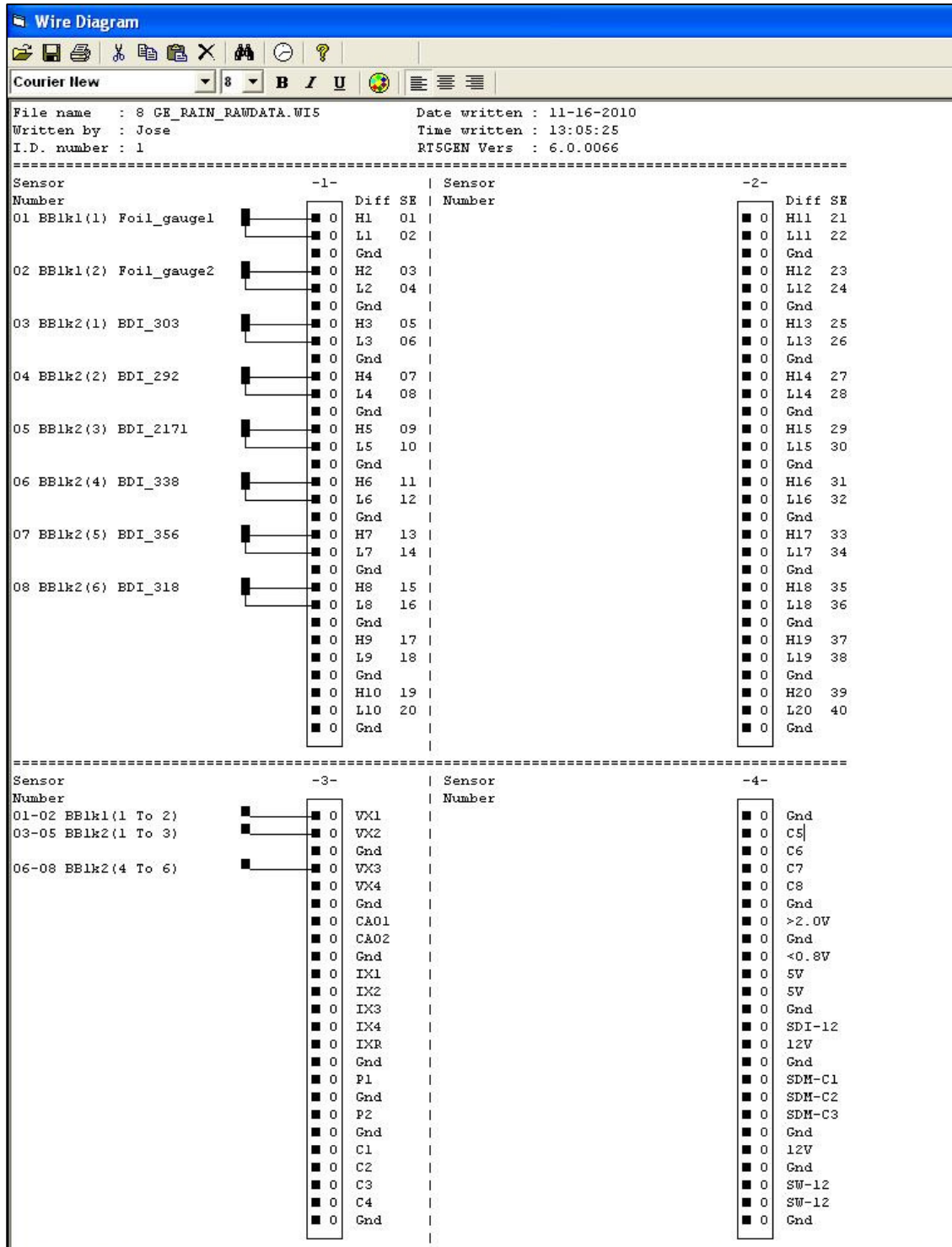
Next Scan

EndProg

'Loop up for the next scan

'Program ends here

\*\*\*\*\* Program End \*\*\*\*\*



## **APPENDIX C. HISTROGRAMS AND DATA PLOTS**

The complete data set recorded during the in-service monitoring period is presented herein. Rainflow histograms, raw data at 100Hz, and minute-based minimum/maximum values are presented for each gage.

